ACS SENSORS

pubs.acs.org/acssensors

Review

Present and Future of Emerging Catalysts in Gas Sensors for Breath Analysis

Published as part of ACS Sensors special issue "Breath Sensing".

Jong Won Baek, Euichul Shin, Jinho Lee, Dong-Ha Kim, Seon-Jin Choi,* and Il-Doo Kim*

Cite This: *ACS Sens.* 2025, 10, 33−53

Read Online

ACCESS | Metrics & More | Article Recommendations

ABSTRACT: To rationalize the noninvasive disease diagnosis by breath analysis, developing a high-performance gas sensor with exceptional sensitivity and selectivity is important to detect trace biomarkers in complex exhaled breath under harsh conditions. Among the various technological innovations, catalyst design and synthesis techniques are the foremost challenges, because gas sensing properties are predominantly determined by surface chemical reactions governed by catalytic activities. Conventional nanoparticle-based catalysts, with their simple structural features, have technical limitations in achieving the requirement for accurate breath analysis. Innovative strategies have been pursued to synthesize unconventional catalyst types with enhanced catalytic capabilities. This Perspective provides a comprehensive overview of recent advancements in catalyst technology for chemiresistive-type gas sensors used in breath analysis. It discusses various emerging catalysts, such as doping catalysts, single-atom catalysts (SACs), bimetallic alloy catalysts, high-entropy alloy (HEA) catalysts, exsolution catalysts, and catalytic filter membranes, along with their unique chemical activation mechanisms that enhance gas sensing properties for detecting target biomarkers in exhaled breath. The review also explores novel strategies for catalyst design, including computational prediction, advanced synthesis techniques, and the integration of sensor arrays with artificial intelligence (AI) to improve diagnostic reliability. By highlighting the crucial role of these emerging catalysts, this review provides valuable insights into the catalytic, synthetic, and analytical aspects that are essential for advancing breath analysis technology.

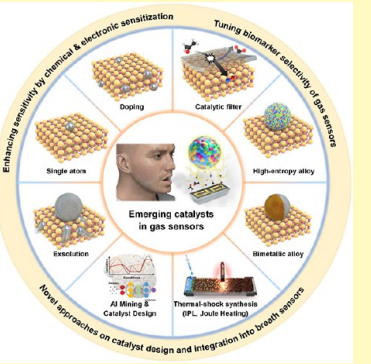

KEYWORDS: *catalyst, gas sensor, breath analysis, biomarker, diagnosis*

BIOMARKERS FOR BREATH ANALYSIS & DISEASE DIAGNOSIS

Breath analysis offers a powerful and fast diagnostic approach by detecting biomarkers in human exhaled breath, which can diagnose various diseases by noninvasive tests. The biomarkers, specific volatile organic compounds (VOCs) exhaled during metabolic processes, play a critical role in modern medicine.[1] These chemical signatures can reflect underlying physiological or pathological conditions, enabling the early detection and continuous monitoring of diseases. The field of breath analysis has evolved significantly from basic medical observations to incorporating breath analyzing platforms with advanced gas sensors.[2] With the advancements in gas sensor technology, breath analysis has become more precise in detecting trace amounts of biomarkers, opening new opportunities for healthcare applications. In particular, the development of Internet of Things (IoT) technology promotes the integration of gas sensors into portable health kits and mobile devices for personal health monitoring.[3] Therefore, the development of highly sensitive and selective gas sensors is becoming increasingly important for fast and accurate disease diagnosis by continuous monitoring of the sensing data.

Various diseases are associated with distinct breath biomarkers, offering the potential to diagnose specific diseases with gas detection. For instance, halitosis is associated with VOCs or volatile sulfuric compounds (VSCs) such as hydrogen sulfide (H_2S), methyl mercaptan (CH_3SH), and dimethyl sulfide (C_2H_6S), which helps assessment of either intraoral or extra-oral health.[4] Asthma involves a major biomarker of nitric oxide (NO), where continuous monitoring of NO levels using gas sensors can aid disease management.[5] Similarly, acetone (C_3H_6O) levels in the exhaled breath can serve as a biomarker for type I diabetes, as well as the acetone levels are closely related to fat-burning metabolism, offering

Received: September 11, 2024
Revised: October 20, 2024
Accepted: November 5, 2024
Published: November 25, 2024

https://doi.org/10.1021/acssensors.4c02464
ACS Sens. 2025, 10, 33−53

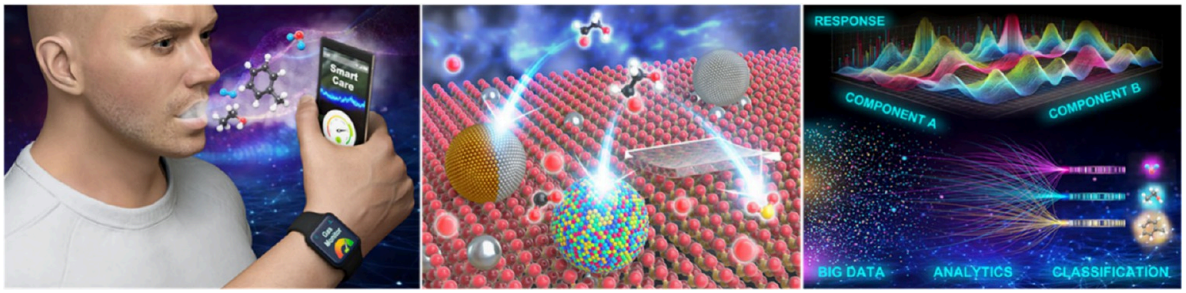

Figure 1. Emerging catalysts and gas sensors for application in breath analysis.

potential feasibility for monitoring the progression of diabetic symptoms.[6] In addition, exhaled isoprene (C_5H_8) gas can reflect metabolic byproducts or blood cholesterol levels.[7,8] In lung cancer, exhaled breath contains VOCs such as benzene (C_6H_6) and toluene (C_7H_8).[9] Early detection and screening through gas sensors for cancer diagnosis can significantly improve the survival rates of cancer patients. Effective gas detection, especially under challenging conditions, requires the ability to detect target gases at parts-per-billion (ppb) to parts-per-trillion (ppt) levels while maintaining long-term stability and ensuring selectivity against other biomarkers. This is crucial even in high concentrations of interfering substances, such as water vapor (H_2O), as exhaled breath typically contains 80−90% relative humidity (RH).

GAS SENSORS FOR BREATH ANALYSIS

Breath biomarkers offer a promising breakthrough for the rapid and noninvasive diagnosis of various diseases. Since the diagnostic accuracy of breath diagnosis relies on the identification and quantification of gaseous biomarkers in human exhaled breath, the development of high-performance gas sensors is essential for enhancing the accuracy of breath analyzers. Among the various types of gas sensors, chemiresistive gas sensors offer fast responding time with adequate detection limits, making them particularly suitable for breath analysis.[10−12] Additionally, chemiresistive sensors are preferred for portable electronic devices due to their simple fabrication processes and nanoscale miniaturization, utilizing a wide range of nanomaterials such as metal oxides,[13−23] transition metal chalcogenides,[24−26] and carbon-based materials.[27,28] The incorporation of catalytic materials with these sensing materials is crucial for enhancing sensitivity and selectivity by accelerating surface chemical reactions and charge transfer processes.[29,30] Noble metals (e.g., Au, Ag, Pt) and heterogeneous metal oxide nanoparticles (NPs) have been generally employed as catalysts, providing superior sensitivity to VOCs at parts-per-million (ppm) levels for applications in air quality monitoring. Nevertheless, new approaches in the design and synthesis of innovative catalysts are necessary for gas sensors as detecting specific biomarkers in exhaled breath is more challenging. Human exhaled breath contains a complex mixture of gases, often with high concentrations of humidity, interfering precise identification of target biomarkers.[2] Also, the extremely low concentrations at parts per trillion levels in exhaled breath require high sensitivity with superior gas discrimination ability to identify similar molecular structures of biomarkers. Therefore, substantial advancements in gas sensing catalysts are still required to address the demands of breath analysis. Accordingly, numerous synthetic methods for developing novel catalysts are being explored, requiring a comprehensive understanding of emerging catalysts for gas sensors used in breath analysis. While several review articles cover the gas sensors for breath analysis, they mainly focus on sensing materials or sensor design, lacking insights from the catalyst perspective.[31−33]

In this Perspective, recent advances in novel catalyst technology for chemiresistive gas sensors are presented, highlighting the innovative approaches for catalyst design, synthesis, and characterization for biomarker detection capability (Figure 1). The fundamental gas sensing and catalytic sensitization mechanisms are initially outlined to identify key design parameters for emerging catalysts. Subsequently, various synthetic methods for novel catalysts, including doping catalysts, single-atom catalysts (SACs), bimetallic alloy catalysts, high-entropy alloy (HEA) catalysts, exsolution catalysts, and catalytic filter membranes are discussed in conjunction with their biomarker sensing performance. Moreover, design strategies for novel catalysts and sensor devices are explored, incorporating computational methods and thermal-shock processes. These include catalyst design for the highly active gas sensors with active learning-based computational calculations. Finally, future directions for breath analysis and noninvasive diagnostic platforms are proposed, emphasizing catalyst design challenges and innovations in catalyst incorporation into sensing materials by identifying the current state of catalyst development in gas sensors.

MECHANISM OF GAS SENSORS AND CATALYTIC EFFECT

Basic Principles in Chemiresistive Gas Sensors. This review primarily focuses on the role of catalysts in chemiresistive gas sensors developed for breath analysis. The fundamental operating principle of chemiresistive sensors involves measuring changes in the electrical resistance of the sensing layers caused by the interactions between oxygen species (O_2^-, O^-, and O^{2-}) adsorbed from the atmosphere and various target gases, including a range of biomarkers.[29,34] These interactions involve physical adsorption (physisorption), chemical adsorption (chemisorption), and forming or eliminating surface and bulk defects within the sensing layers. Among these mechanisms, the chemisorption of oxygens is particularly important in most semiconducting metal oxide-based gas sensors, especially operating at elevated temperatures, typically between 100 and 500 °C.[35,36] At these operating temperatures, a larger amount of adsorbed oxygen species increases the number of reaction sites available for the target gas, thereby significantly enhancing the sensitivity and overall performance of the sensors. On the other hand, semiconducting metal oxide-based sensors have two operating

https://doi.org/10.1021/acssensors.4c02464
ACS Sens. 2025, 10, 33−53

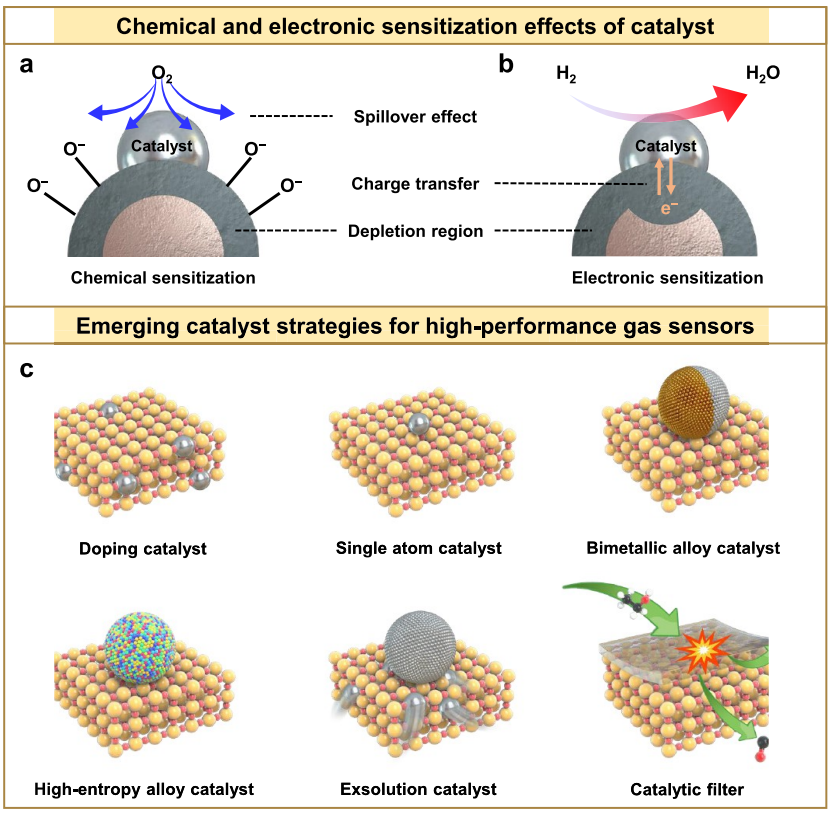

Figure 2. Schematic illustration for (a) chemical sensitization, (b) electronic sensitization of catalyst, and (c) emerging catalyst systems, including doping catalyst, single-atom catalyst, bimetallic alloy catalyst, high-entropy alloy catalyst, exsolution catalyst, and catalytic filter.

functions: receptor function and transducer function.[37] The receptor function represents the surface reactivity of the sensing layer with the gas molecule, which involves identification of the target gas. The transducer function then converts these surface chemical phenomena into measurable signals in the electrical resistance of the sensor.[38] Among these, the superior sensing performance for detecting and discriminating biomarkers can be attributed to enhanced receptor functions. It is widely accepted that negatively charged oxygen species (O_2^-, O^-, and O^{2-}) form depletion layers (for n-type metal oxides) at the surface, which react with target biomarkers, leading to electrical resistance changes upon the modulation of depletion layer thickness.[39] Therefore, it has been challenging to discriminate target biomarkers due to similar gas reaction processes of different gas types with adsorbed oxygen species. The receptor function determines the surface affinity of sensing layers to target gases, which assigns the gas selectivity from the diverse target gases. Importantly, catalytic sensitizers distributed on the sensing layers are crucial to controlling the surface properties of sensing layers affecting the selectivity and improving the sensing performance by influencing these basic functions through various mechanisms.

Catalyst-based Gas Sensing Mechanism. The operating mechanism of chemiresistive gas sensors predominantly occurs at the gas−solid interface, making receptor function vital. It is well-established that the chemical adsorption and reaction of gas analytes on the surfaces of metal oxides require activation energy. Therefore, by precise control of the composition and morphology of functionalized catalysts, the receptor function can be optimized to lower the activation energy and promote specific gas adsorption, thereby enhancing gas selectivity and sensitivity. Catalysts for gas sensors enhance sensing performance based on the sensitization effect through two mechanisms.[40] First, the chemical sensitization effect, also known as the spillover effect, promotes the adsorption of specific gas molecules on the sensor surface by lowering the activation energy of adsorption, often facilitating oxidation or reduction reactions (Figure 2a).[41] This effect involves the adsorption of the gas molecule and the migration of ionic adsorbate to the surface of the sensing layers. As the chemical sensitization effect relies on the specific interaction between the catalyst surface and the gas molecule, the chemical sensitizer can effectively control the selectivity of the gas sensor. By improving selectivity, chemical sensitizers ensure the sensor can accurately detect biomarkers in complex environments, such as human breath,[42] where various VOCs are present. On the other hand, electronic sensitizers modulate the electronic properties of the sensing layers, affecting charge carrier concentration, electrical conductivity, and electronic energy band structure (Figure 2b).[43] This modulation boosts the signal transduction of sensing layers induced by gas reaction (transducer function), resulting in an enlarged gas response value. This electronic sensitization effect is based on the electronic interaction between the catalyst and the sensing layer. Therefore, selecting an appropriate combination of catalyst and base sensing material systems is important to maximize the electronic sensitization effect. Together, chemical and electronic sensitizers enhance both the response and the selectivity of the sensor, making them vital for advanced gas sensing technologies for breath analysis.

To date, noble metal catalysts have been incorporated into gas sensors with their sensitization effects.[44] However, the current gas sensing performance with conventional NP-type catalysts is insufficient to meet the requirements of practical

https://doi.org/10.1021/acssensors.4c02464
ACS Sens. 2025, 10, 33−53

breath analyzer applications such as gas discrimination ability to various biomarkers in sub-ppb concentrations, reliable gas detection under high humidity conditions, and long-term stability under harsh operating conditions. These limitations are primarily attributed to their simple NP morphology, which restricts catalytic efficiency, even with nanoscale dimension. The NPs inevitably possess internal atoms that do not contribute to the catalytic activity, reducing the catalyst loading efficiency. Moreover, the weak interaction between metal catalysts and support sensing materials, typically metal oxides, leads to catalytic performance degradation under harsh operating conditions due to aggregation by atomic migration or poisoning effect at the catalyst surface.[45] Additionally, the simple single-element composition exhibits low gas selectivity over the range of similar gas species, hindering the precise detection of specific biomarkers.

To address these limitations, recent innovations have emerged, including doping catalysts,[46] SACs,[47] bimetallic alloy catalysts,[48] HEA catalysts,[49] exsolution catalysts,[50] and catalytic filter membranes (Figure 2c).[51] Doping involves introducing specific atoms to alter the electronic properties of the sensing materials, enhancing their sensing performance and surface activity.[52,53] SACs consist of isolated metal atoms supported on a material, which maximizes catalytic efficiency and surface area, resulting in highly sensitive and consistent gas detection.[54] Bimetallic alloy catalysts have a diverse array of properties stemming from each element. These alloy catalysis are remarkable because of the unexpected synergistic effects that arise when different elements interact.[55] HEA are composed of multiple elements in nearly equal amounts, providing increased stability and resistance to degradation, which enhances their durability and performance in harsh conditions.[56] Exsolution catalysts are formed through the spontaneous growth of metal NPs on the surface of a host oxide.[57] In this process, certain cations doped in a complex oxide lattice selectively diffuse to the surface and grow to NPs when the oxide is partially reduced at high temperatures, remaining firmly anchored to the lattice. The anchoring of exsolution catalysts ensures their stability under high temperatures and harsh conditions, unlike that of conventional NPs, and enhances the durability of gas sensors. Catalytic filter membranes act as a pretreatment stage by either blocking the diffusion of interfering gases through chemical binding or converting less-reactive gases into more-reactive ones, thereby enhancing selectivity.[58] This process improves the reliability of measurements in complex gas mixtures such as exhaled breaths. Advanced catalysts facilitate selective chemical reactions between catalysts and biomarker target gases and effectively modulate the electronic conductivity of the sensing layers, enhancing the sensing performance for breath analysis. In the next section, we will discuss more detailed features and advantages of each type of catalyst for potential use in exhaled breath sensors.

EMERGING CATALYSTS IN GAS SENSORS

In this section, we provide an overview of the emerging catalysts for gas detection under extremely harsh conditions, including the detection of target gases at parts per trillion levels, long-term stability, and selectivity against other biomarkers in the presence of highly interfering humid conditions. We will discuss not only the effect of electronic and chemical sensitizations of these catalysts but also their stability, catalytic efficiency, and electronic structure engineering of host metal oxides.

Doping Catalysts. Introducing single-atom catalysts or heteroatom doping into sensing materials are effective strategies for enhancing gas sensing properties, as they can significantly improve both sensitivity and selectivity.[47,54,59] Catalysts accelerate surface reactions in gas sensing layers through chemical or electronic sensitizations, thereby boosting the sensitivity to target gases.[60] Similarly, heteroatom doping in sensing materials such as graphene,[59,61,62] hollow carbon supports,[63] metal oxides,[64] and conjugated polymers[65,66] not only modulates the electronic properties of these materials but also introduces various active sites that facilitate gas adsorption and dissociation.

In general, doping in metal oxides with an element that has an oxidation state lower than that of the host metal introduces additional oxygen vacancies to maintain charge neutrality. These surface oxygen vacancies significantly influence the concentration of adsorbed oxygen species, which directly affect both the conductivity of the sensing material and its gas adsorption capacity.[67,68] Conversely, doping with an element with a higher oxidation state leads to the formation of metal vacancies. The degree of lattice mismatch during doping should also be considered, as these lattice distortions can alter the surface geometry and bonding in metal oxides, affecting adsorption energies and overall sensing performance.[69,70] Thus, the type and concentration of the dopant play critical roles in determining the degree of conductivity modulation and overall sensor performance.

In carbon-based materials, doping alters the electrical conductivity by shifting the Fermi level and modifying the density of states near the Dirac point.[71,72] For example, when an n-type dopant is introduced into graphene, it donates additional electrons to the graphene lattice, shifting the Fermi level closer to the conduction band, reducing the number of holes, and thereby decreasing the conductivity of p-type sensing materials.[73]

Doping not only effectively modulates electrical conductivity but also creates active sites for the adsorption and reaction of gas molecules, directly influencing the sensor performance. This improvement can be attributed to the increased number of active sites, enhanced catalytic activity, and improved gas adsorption. The integration of SACs further refines this process by providing atomic-level precision in catalysis, ensuring that each gas molecule interacts with highly reactive and tailored sites. Introducing doping and/or SACs allows for the fine-tuning of gas sensors, enabling rapid, sensitive, and selective detection of gases at low concentrations, which is critical for applications in medical diagnostics and healthcare.[47]

Single-Atom Catalysts (SACs). Single-atom catalysts exhibit high reactivity due to their atomic-scale distribution on support sensing materials.[74,75] However, stabilizing SACs on nanostructures with high loading amounts and uniformity has been challenging. To address this issue, Shin et al. reported the stabilization of Pt single atoms on SnO_2 nanofibers (NFs) using a carbon nitride and SnO_2 heterojunction trapping strategy.[76] Pt SACs anchored on melamine-derived carbon nitrides (Pt-MCN) were synthesized by exfoliating carbon nitride nanosheets (NSs) and subsequently using a wet impregnation method to anchor the Pt SACs with a high loading amount (4.3 wt %). The as-synthesized Pt-MCN was then loaded onto the SnO_2 nanotubular structure by using electrospinning, followed by a subsequent calcination process

https://doi.org/10.1021/acssensors.4c02464
ACS Sens. 2025, 10, 33−53

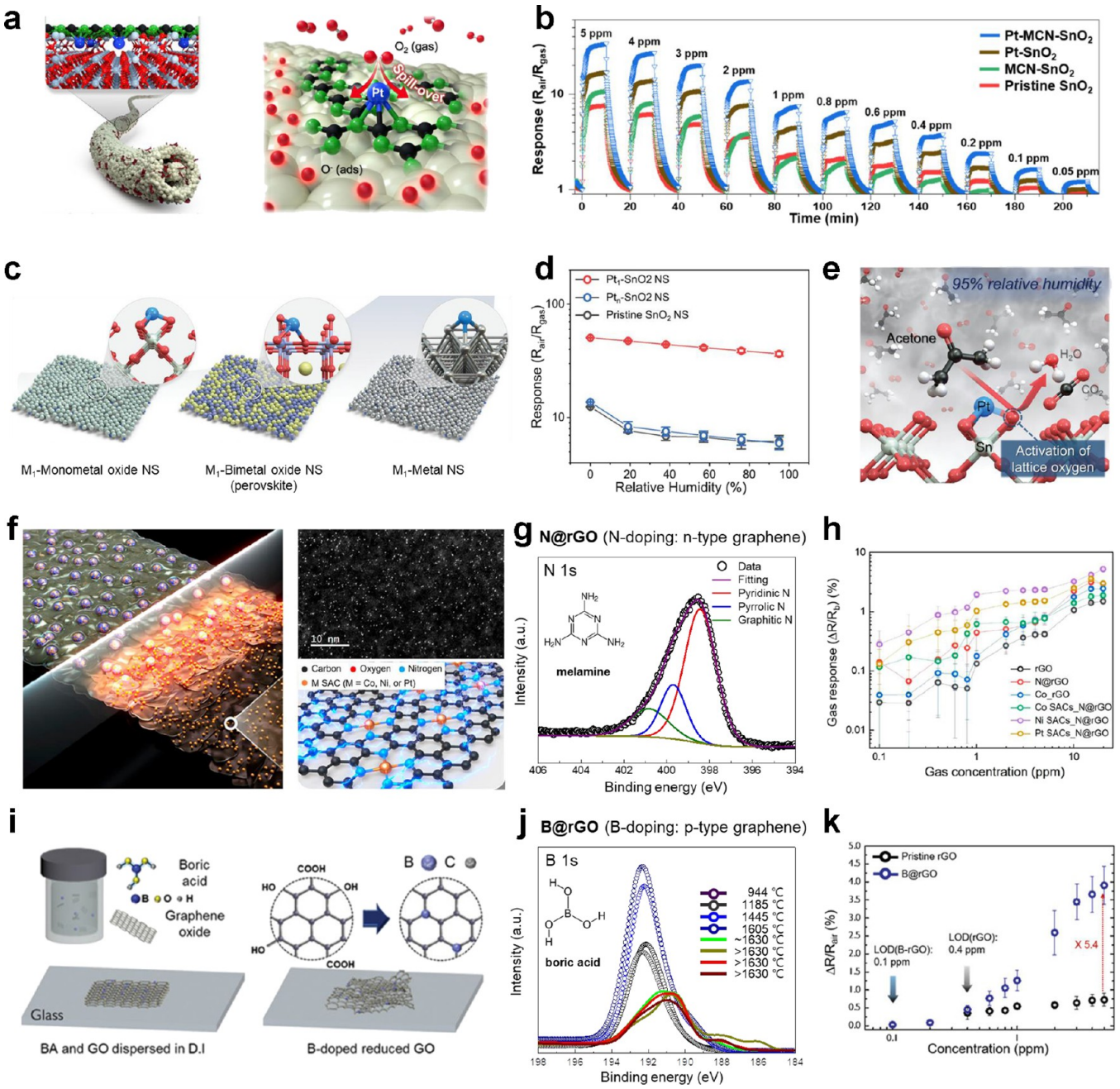

Figure 3. (a) Schematic illustration of Pt SAC-SnO_2 nanofibers and oxygen dissociation over Pt SAC and (b) dynamic response transitions toward HCHO. Reproduced with permission from ref 76. Copyright 2020 American Chemical Society. (c) Synthetic schematic illustration of SAC on nanosheets, (d) effect of humidity on the sensing response under 5 ppm of acetone, and (e) sensing mechanism of SAC under highly humid conditions. Reproduced with permission from ref 77. Copyright 2022 Wiley-VCH GmbH. (f) Synthesis schematic illustration of N doped rGO (N@rGO) by an ultrafast flash-thermal shock technique, (g) N 1s XPS spectrum of N@rGO, and (h) sensing response transitions toward various concentrations of NO_2. Reproduced with permission from ref 82. Copyright 2023 American Chemical Society. (i) Schematic illustrations of processing for B doping on GO (B@rGO), (j) B 1s XPS spectrum of B@rGO, and (k) sensing response transitions toward various concentrations of NO_2. Reproduced with permission from ref 83. Copyright 2020 Wiley-VCH GmbH.

(Figure 3a). This structure is advantageous for gas sensing layers due to its high surface area, well-developed porosity, and the catalytic effects of the Pt-MCN complexes. To demonstrate the effectiveness of the Pt-MCN complex catalysts for formaldehyde (HCHO) sensing, four different sensors were prepared: pristine SnO_2, MCN-loaded SnO_2, Pt-doped SnO_2, and Pt-MCN-functionalized SnO_2 (Figure 3b). The results showed that doping SnO_2 with Pt atoms improved the HCHO response, while MCN loading alone did not significantly enhance the sensing properties. Notably, the Pt-MCN-loaded SnO_2 sensor exhibited superior sensing performance with the responses (R_{air}/R_{gas}) of 33.9 and 1.5 at 5 and 5 ppb, respectively, attributed to the synergistic effects of SnO_2-MCN heterojunction formation and the maximized catalytic efficiency achieved through atomic isolation of Pt. The Pt−N/C sites in Pt-MCN provide strong adsorption sites for O_2, dissociating into chemisorbed oxygen (e.g., O^-) on the SnO_2 sensing layers via a spillover process. Because the Pt SACs are

https://doi.org/10.1021/acssensors.4c02464
ACS Sens. 2025, 10, 33−53

encapsulated between carbon nitride and SnO_2, the sensors exhibited exceptional long-term cycling stability over 27 repeated cycles with high resistance to sintering over 2 months, even at a high operating temperature of 275 °C.

The introduction of high-density SAC functionalization on other dimensional nanostructures, such as 2D NS structures, holds significant potential for creating diverse high-performance gas sensing materials. In this context, Shin et al. demonstrated a general method for preparing SACs on metallic, metal oxide, and perovskite NSs using N-doped graphene as a sacrificial template to confine the SACs.[77] Specifically, Pt single-atom-stabilized N-doped graphene (Pt_1−NGr) was synthesized by pyrolyzing ethylenediaminetetraacetic acid disodium salt dehydrate (EDTA-2Na·$2H_2O$). Subsequently, various metal precursors were coated onto Pt_1−NGr via a solution-mediated adsorption process, followed by calcination, during which the NGr decomposed, and the metal precursors were oxidized into metal oxide or perovskite structures (Figure 3c). To produce metallic NSs, an additional reduction step was conducted in a H_2/N_2 environment. High-angle annular dark-field scanning transmission electron microscopy (TEM) images demonstrated that Pt single atoms were finely distributed and anchored on SnO_2, $LaCoO_3$, and Pd NSs, respectively. When an excessive amount of Pt precursor was introduced during the synthesis of Pt-anchored N-doped graphene (Pt_n-NGr), Pt nanocluster-functionalized SnO_2 (Pt_n-SnO_2), $LaCoO_3$ (Pt_n-$LaCoO_3$), and Pd NSs (Pt_n-Pd) were obtained.

When sensors are used for breath analysis, it is crucial that the sensors exhibit a stable response, even under highly humid conditions (85−95% RH). Typically, metal oxide-based gas sensors suffer from significant performance degradation in high humidity, as the adsorption of water molecules competes with oxygen chemisorption. In this regard, the sensing properties of pristine SnO_2 NSs, Pt_n-SnO_2 NSs, and Pt_1−SnO_2 NSs were investigated toward 5 ppm acetone gas under various relative humidity conditions (0−95% RH) (Figure 3d). The pristine SnO_2 NSs and Pt_n-SnO_2 NSs displayed degraded sensing responses as the relative humidity increased during acetone sensing. Interestingly, Pt_1−SnO_2 NS sensors exhibited stable sensing properties under highly humid (95% RH) conditions with a response of 95.4 at 10 ppm of acetone. Under high humidity, high-valent Pt species (e.g., Pt surface-doped SnO_2) enhance the reaction between lattice oxygen and reducing gases (e.g., acetone) (Figure 3e). This mechanism activates lattice oxygen near Pt single atoms (Pt−O−Sn boundaries) to react with target gases rather than relying on chemisorbed oxygen. In contrast, Pt_n−SnO_2 NSs, which contain more metallic Pt nanoclusters/NPs, showed about 56.6% reduction in response at 10 ppm of acetone compared to Pt_1−SnO_2 NSs due to NP deactivation under high humidity.

The stabilization of single atoms offers significant advantages not only in metal oxide-based inorganic supports but also in graphene-based sensing materials. In addition, doping plays a critical role in modulating electrochemical properties by inducing n- or p-type effects, while also creating active sites for enhanced gas adsorption through stronger binding energies between doped sites and gas analytes. These strategies include various methods such as chemical vapor deposition using organic precursors,[73] plasma treatment,[78,79] and chemical doping via reactions between graphene and nitrogen-containing compounds.[80,81] However, these approaches typically require prolonged exposure to a reducing atmosphere and elevated temperatures to effectively reduce graphene oxide and achieve heteroatom doping. Therefore, the development of alternative ambient-air and rapid processing methods with high mass productivity is crucial for commercialization.

Recently, Kim et al. introduced an ultrafast flash-thermal shock (FTS) technique that facilitates the efficient and cost-effective production of single-atom-stabilized N-doped graphene (SACs_N@rGO) in an ambient-air environment (Figure 3f).[82] Melamine serves as the N-doping source, enabling thermodynamically stable single-atom sites via metal−nitrogen bonding, resulting in a uniform and high-density distribution of SACs, including Co, Ni, Pt, and Co−Ni dual components. The process involves the self-assembly of melamine on graphene oxide due to zeta potential differences, followed by a single flashlight irradiation that induces a rapid temperature increase to 2850 °C within 10 ms. X-ray photoelectron spectroscopy (XPS) analysis confirmed the degree of N-doping and the reduction of graphene oxide, with nitrogen predominantly doping into pyridinic sites, which is advantageous for catalytic efficiency (Figure 3g).

When metal precursors are included, the FTS process simultaneously stabilizes metal SACs through three key steps: reduction of graphene oxide, N-doping, and SAC anchoring via metal−nitrogen bonding, i.e., M-N_4. Testing with nitrogen dioxide (NO_2) sensors revealed that N-doping improves gas response by creating preferential adsorption sites, while SAC stabilization, especially with Ni, further enhances the response due to higher binding energy between Ni−N_4 sites and NO_2 (Figure 3h). Moreover, N-doping increases electrical conductivity, while SAC anchoring introduces active sites that accelerate the adsorption and dissociation of NO_2 gas, collectively improving the reaction kinetics. For example, Ni SACs_N@rGO showed 7.7-fold and 3.5-fold improved adsorption and desorption rate constants compared to N@rGO, respectively. Overall, the SACs_N@rGO system exhibited excellent sensing characteristics, including response, reversibility, and reaction rates, driven by the combined effects of doping and SACs on the physicochemical properties of rGO systems.

Another study tackled the challenge of achieving low-thermal-budget heteroatom doping and reduction of graphene oxide in ambient air by utilizing flash irradiation of boric acid on graphene oxide with intense pulsed light to synthesize B-doped reduced graphene oxide (B@rGO) (Figure 3i).[83] Boric acid served as the boron doping source, with the photothermal temperature playing a crucial role in effectively decomposing boric acid and facilitating doping on reduced graphene oxide. Given that boric acid vaporizes around 400 °C and graphene oxide reduces between 500−1200 °C, temperatures exceeding 1400 °C were necessary to activate boron doping on reduced graphene oxide. The doping states of boron included BCO_2, BC_2O, BC_3, and BC_4, with their relative compositions varying depending on the photothermal annealing temperature (Figure 3j). Specifically, as the photothermal temperature increased to 1400 °C, the intensity of the BCO_2-related peaks in the B 1s spectra also increased. At temperatures above 1630 °C, BCO_2-related peaks decreased sharply, while BC_4-related peaks became prominent. This work demonstrated the fine-tuning of B-doping states through millisecond-scale, temperature-dependent bond engineering based on the photothermal effects of graphene oxide.

To validate the practical application of B@rGO in chemiresistive sensing, NO_2 sensing tests were conducted

https://doi.org/10.1021/acssensors.4c02464
ACS Sens. 2025, 10, 33−53

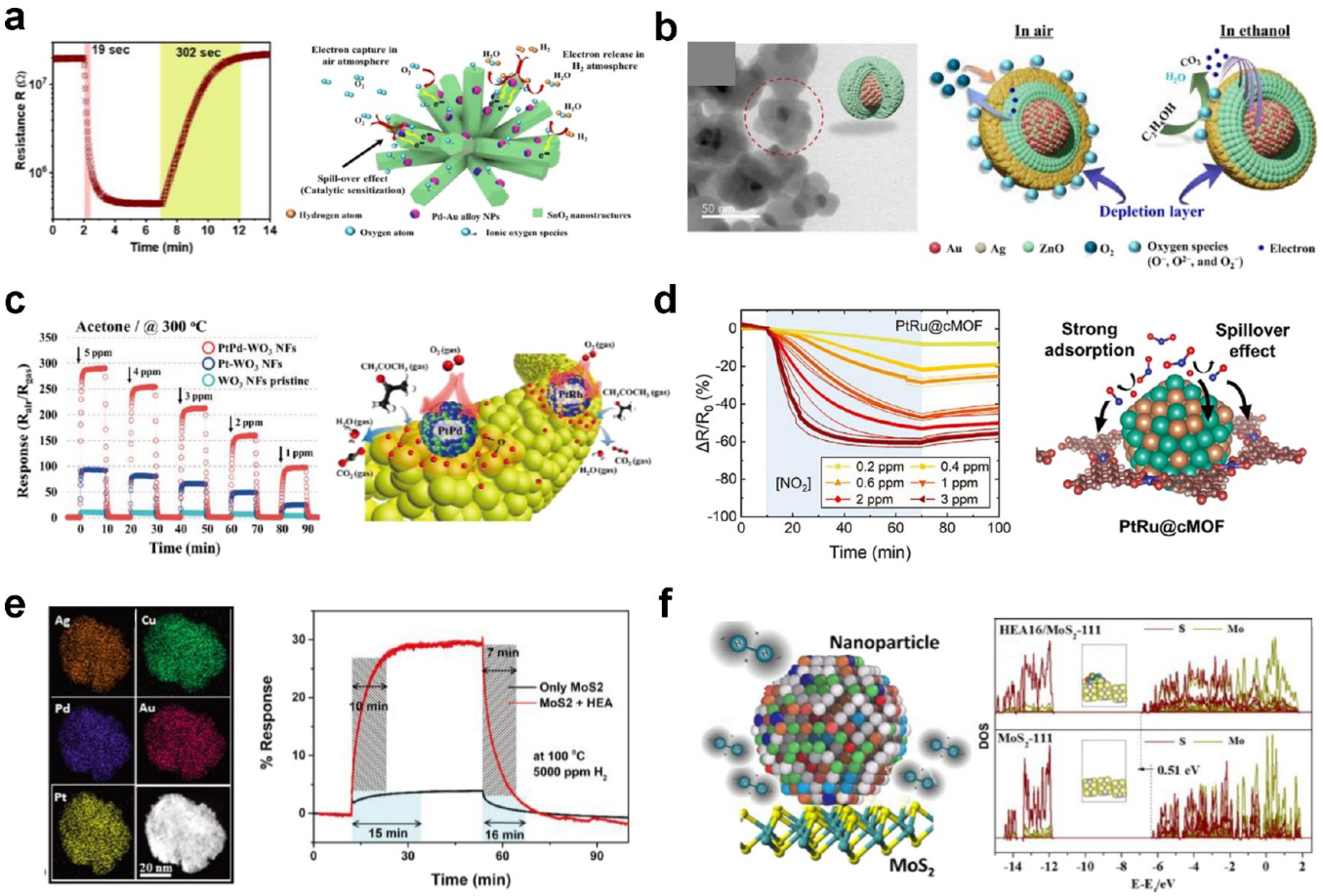

Figure 4. (a) Transient sensing response of bimetallic PdAu alloy catalysts on SnO_2 and their schematic illustration for the sensing mechanism. Reproduced with permission from ref 89. Copyright 2023 Royal Society of Chemistry. (b) TEM image of core−shell NPs, featuring a AuAg alloy as the core and ZnO as the shell, and schematic illustration of ethanol sensing mechanism. Reproduced with permission from ref 91. Copyright 2022 Elsevier. (c) Dynamic acetone sensing response of bimetallic PtPd and PtRh alloys loaded WO_3 NFs and schematic illustration for gas sensing mechanism. Reproduced with permission from ref 42. Copyright 2017 Wiley-VCH GmbH. (d) Response curves of bimetallic PtRu alloy on cMOF toward NO_2, and schematic illustrations for the catalytic effect, including the spillover effect of Pt and strong adsorption for NO_x of Ru. Reproduced with permission from ref 94. Copyright 2021 Wiley-VCH GmbH. (e) Energy-dispersive X-ray spectroscopy (EDS) elemental mapping, scanning transmission electron microscopy (STEM) images of AgAuPtPdCu HEA NPs, and response curve of MoS_2 and HEA-decorated MoS_2 toward 5000 ppm of H_2 at 100 °C. Reproduced with permission from ref 99. Copyright 2020 Royal Society of Chemistry. (f) Schematic illustration of hydrogen adsorption on TiZrVNbHf HEA NPs decorated MoS_2, and DOS of MoS_2 and HEA NPs decorated MoS_2 systems. Reproduced with permission from ref 100. Copyright 2023 Royal Society of Chemistry.

and compared with pristine rGO sensors (Figure 3k). The B@rGO sensors showed a 5.4-fold improvement in response ($\Delta R/R_{air}$ = 3.8%) to 5 ppm of NO_2 compared to the response ($\Delta R/R_{air}$ = 0.7%) of pristine rGO, attributed to the presence of B-doping active sites in the graphene lattice. These B-doped active sites, including BC_3, BCO_2, and BC_2O, provide strong binding sites for NO_2 molecules, enhancing resistance modulation and sensor response. Additionally, B@rGO could detect NO_2 concentrations as low as 0.1 ppm, while the detection limit for pristine rGO was 0.4 ppm. This process allows for large-scale, rapid doping and reduction with a significantly lower thermal budget, resulting in a material with abundant B active sites that is highly effective for sensitive and selective NO_2 sensing at room temperature.

Bimetallic Alloy Catalysts. Bimetallic alloys exhibit a range of properties contributed by each element. Moreover, the unexpected synergistic effects between these elements make these new bimetallic alloy catalysts particularly noteworthy.[84] For instance, in ammonia synthesis, optimal catalytic performance is achieved by balancing two opposing factors: a low activation barrier for N_2 dissociation and a surface with low coverage of adsorbed atomic nitrogen.[85] This balance requires a catalyst with strong and weak N-surface interactions, avoiding extremes of a high or low nitrogen adsorption energy. The Mo, which has high adsorption energy of N, and Co, which has low adsorption energy of N, alloy catalyst was developed into ammonia synthesis catalysts due to their complementary adsorption and desorption of nitrogen in the ammonia synthesis. This catalyst showed significantly higher ammonia synthesis activity than its individual components and even outperformed Fe and Ru, which have high turnover frequencies for ammonia synthesis. Depending on the mixing pattern, bimetallic alloy NPs can be classified into three main types: core−shell structures, heterostructures, and intermetallic or alloyed structures.[84] The synergistic effects of these diverse structures significantly enhance catalytic activity suitable for emerging catalysts in exhaled breath sensors.

Hydrogen gas is a biomarker for gastrointestinal disorders owing to insufficient absorption in the colon by metabolizing carbohydrates, including lactose.[86] Hydrogen gas is easily

https://doi.org/10.1021/acssensors.4c02464
ACS Sens. 2025, 10, 33−53

adsorbed on the Pd surface, forming PdH_x due to the spillover effect of H_2.[87] This process causes volume expansion, which enhances the diffusion and adsorption−desorption rates of gas molecules, leading to improved sensitivity through a large change in the resistance. However, at temperatures above 300 °C, commonly used in gas sensor systems, the Pd catalyst tends to oxidize to PdO. Additionally, repeated volume changes can cause cracking and delamination of the Pd catalyst. To address these limitations, Pd-based alloys have been explored to improve hydrogen gas sensing performance through the restriction of deactivation of Pd.[88−90] Among these alloys, Au is often incorporated into Pd due to its equal face-centered cubic crystal structure, which helps maintain structural integrity during continuous hydrogenation and dehydrogenation cycles. The atomic-level electrical interaction between Au and Pd further amplifies the sensitization effect. In addition, the Au can prolong the lifetime of the heat-generated hole−electron pairs due to high work function compared to support metal oxides and has a strong capability to dissociate oxygen molecules to enrich the activated oxygenic species. Moreover, the Schottky barrier between the PdAu alloy and the supporting metal oxides promotes electron transfer, creating an additional depletion layer. As a result, PdAu alloys exhibit improved gas adsorption, dissociation, and activation properties, as evidenced by a large resistance change (R_{air}/R_{gas} = 46.4) toward 100 ppm of H_2 at 175 °C with fast response time (19 s) (Figure 4a).

Similar to the prevention of Pd oxidation by alloying with Au, an AgAu alloy has been developed to inhibit Ag oxidation. However, the density of atomic oxygen decreases as the Au content increases since the additional electrons in the antibonding orbitals of Au weaken the binding of the atomic oxygen Ag−O bond on the alloy surface. Thus, a suitable combination of highly active Ag and Au, which can enhance the stability, is required to improve the gas sensing performance. As a result, the $Ag_{70}Au_{30}$ alloy exhibited high sensing performance toward ethanol (Figure 4b).[91] In addition, Pt-based alloy catalysts play a crucial role in accelerating the dissociation of oxygen molecules and target gases through a spillover process. The inhomogeneity of the Pt_3Co surface creates nonequivalent adsorption sites, increasing the amount of oxygen adsorption species.[92] The adsorbed oxygen molecules then dissociate along the lowest energy barrier pathways. While Pt-centered pathways have less stable transition states and higher activation energies, Co-centers are more reactive for O_2 dissociation. As a result, the Pt-based alloy exhibits a high oxygen spillover effect due to the abundance of oxygen adsorption sites and the low activation barrier for O_2 dissociation.

Kim et al. reported the synthesis of highly acetone-sensitive WO_3 NFs with Pt-based bimetallic NPs, including Pd and Rh.[42] Taking advantage of nanoscale protein cavities in the apoferritin, the high specific area of small size (less than 3 nm) and dispersibility of Pt-based alloys improved the gas sensing performance. PtPd and PtRh NPs not only enhance the dissociation of molecular oxygen and the analyte but also contribute to increased depletion widths through the formation of p−n junctions between n-type WO_3 and p-type PtO_x, Rh_2O_3, and PdO on the surface (Figure 4c). This interaction increased the baseline resistance, leading to more significant resistance changes and enhanced sensitivity with responses (R_{air}/R_{gas}) of 97.5 and 104 toward 1 ppm acetone at 300 °C, with the decoration of PtPd and PtRh on WO_3 NFs, respectively.

A catalytic Ru promotes the adsorption of nitrogen-containing molecules, transforming its oxidation state from Ru^{4+} to Ru^{3+}.[93] Park et al. demonstrated the NO_x adsorption capabilities of a PtRu catalyst incorporated into conductive metal−organic frameworks (cMOFs), specifically Cu_3(hexahydroxytriphenylene)$_2$ (Cu_3(HHTP)$_2$).[94] The XPS analysis revealed that the Cu^{2+} peaks in the PtRu@cMOF were shifted to higher binding energies compared to monometallic NPs (Pt@cMOF and Ru@cMOF), indicating that more electrons were depleted of the Cu metal nodes upon NO_2 adsorption, where NO_2 is adsorbed on the Cu open metal sites. As a result, a noticeable sensing response ($\Delta R/R_0$) of −53.0% was obtained with PtRu@cMOF toward 3 ppm of NO_2 at room temperature. The density functional theory (DFT) calculations confirmed that the PtRu catalyst accelerates the dissociation of NO_2, enhances the adsorption of nitrogen molecules at Ru sites, and promotes NO diffusion, leading to improved NO_2 sensing performances (Figure 4d).

High-Entropy Alloy Catalysts. The HEA represents a novel and increasingly significant class of metallic materials, distinguished by their unique compositional and structural properties. Unlike traditional alloys, which typically consist of one or two principal elements with additional elements in minor quantities, HEA is engineered with five or more principal elements, each contributing significantly to the overall composition—typically ranging between 5−35% by atomic percentage.[95] This HEA catalyst can be fabricated under similar conditions to the conventional alloy catalyst synthesis, but precise control of the HEA composition is crucial to stabilize the multielemental system and prevent phase separation, taking into account the thermodynamic stability and lattice structure. This approach results in a highly complex and balanced elemental distribution that sets HEA apart from conventional alloy systems.[96]

Interestingly, the catalytic properties of multicomponent HEA are not the simple addition of the advantages from their individual components, but they have unique catalytic properties with synergistic effects. Notably, HEA NPs have the potential to reduce the amount of noble metals required without sacrificing catalytic efficiency, as these metals can be highly dispersed within the HEA structure. For example, PtPdAuAgCu HEA catalyst containing strong hydrogen adsorption elements (Pd, Pt) with weaker ones (Ag, Au) has been shown to enhance catalytic activity compared to a single-element catalyst for electrocatalysis.[97] This is due to the low free energy of intermediates at the surface of HEA during CO_2 reduction reactions, which promotes the electroreduction of formic acid to produce CO_2 and H_2 even at zero bias. Wang et al. demonstrated the potential of HEA NPs replacing novel metals, such as PtIrCuNiCr and PtAuPdFeNi, for the hydrogen-evolving reaction (HER) and oxygen-evolving reaction (OER) catalyst. The Pt atoms in these HEA NPs induce a lattice distortion, leading to a thermodynamic nonequilibrium state. A higher free energy potential of lattice-distorted HEA NPs lowers the energy barrier of catalytic reactions and enhances catalytic performance.[98]

In the case of gas-sensing catalysts, Kusuma et al. reported the development of a noble metal-based HEA catalyst, AgAuCuPdPt HEA, for hydrogen gas detection.[99] Pd has been a well-known catalyst for a chemical sensitizer toward hydrogen gas, facilitating H_2 dissociation and resistance-driven

https://doi.org/10.1021/acssensors.4c02464
ACS Sens. 2025, 10, 33−53

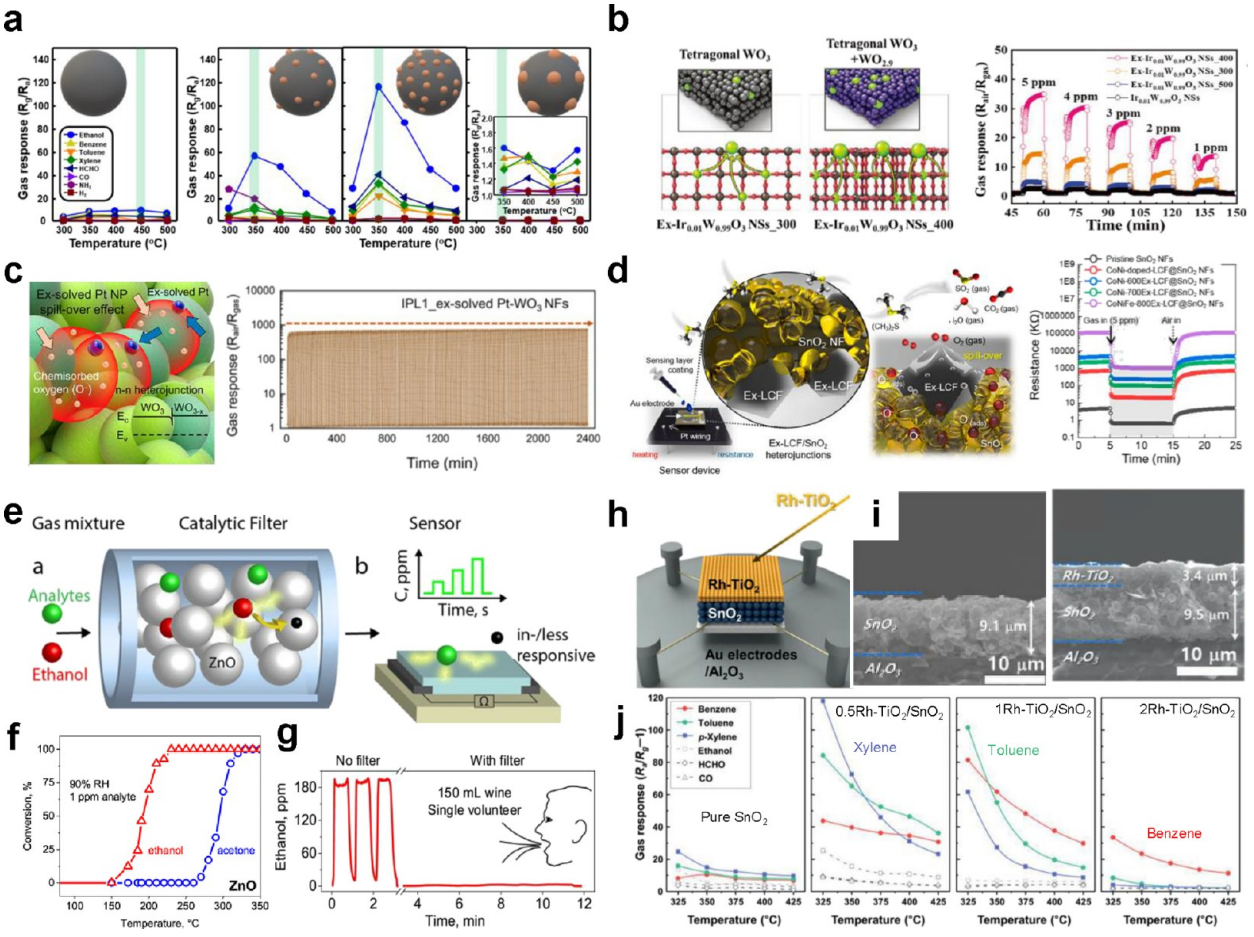

Figure 5. (a) Gas sensing characteristics of LCCoT and exsolved Co-decorated LCCoT toward various gases at 5 ppm in a temperature range of 300−500 °C. Reproduced with permission from ref 106. Copyright 2022 American Chemical Society. (b) Schematic illustrations of exsolution and dynamic sensing responses in a concentration range of 1−5 ppm toward H_2S with Ir doping and Ir exsolution catalysts-decorated WO_3 NSs. Reproduced with permission from ref 107. Copyright 2020 Wiley-VCH GmbH. (c) Synergistic effect of H_2S sensing performances between exsolved Pt and n-n heterojunction of WO_3, and cyclic sensing performance to 1 ppm of H_2S. Reproduced with permission from ref 108. Copyright 2022 American Chemical Society. (d) Schematic illustration of gas sensors and sensing mechanism and resistance transition curves of exsolution catalysts decorated SnO_2 NFs. Reproduced with permission from ref 109. Copyright 2023 American Chemical Society. (e) Schematic illustration of bed-type catalytic filter for ethanol removal. (f) Conversion ratio of 1 ppm of ethanol (red triangles) and acetone (blue circles) on the ZnO bed as a function of the filter temperature. (g) Ethanol concentration of human exhaled breath without and with ZnO filter at 260 °C. Reproduced with permission from ref 58. Copyright 2020 American Chemical Society. (h) Schematic illustration of Rh-TiO_2/SnO_2 gas sensor. (i) Cross-sectional SEM image of SnO_2 and Rh-TiO_2/SnO_2 sensing films. (j) Gas sensing characteristics of pure SnO_2, 0.5Rh-TiO_2/SnO_2, 1Rh-TiO_2/SnO_2, and 2Rh-TiO_2/SnO_2 gas sensors toward 5 ppm of gases (benzene, toluene, *p*-xylene, ethanol, HCHO, and CO) in the temperature range of 325−425 °C. Reproduced with permission from ref 118. Copyright 2021 Wiley-VCH GmbH.

sensing through volumetric expansion. The equiatomic AgAuCuPdPt HEA NPs on MoS_2 exhibited improved H_2 sensitivity, selectivity, and response/recovery times, even with a Pd content of only 20% (Figure 4e). The AgAuCuPdPt HEA NPs induced the reduction of the MoS_2 work function from 4.9 to 4.75 eV due to electron transfer from HEA to MoS_2. This electron transfer increases the resistance of the p-type semiconductor MoS_2 due to enlarged surface oxygen adsorption based on the chemical sensitization effect. This significant rise in oxygen adsorption leads to an enhanced gas sensitivity with a large change in electrical resistance by the gas reaction. The HEA-decorated MoS_2 demonstrated enhanced response and improved response (10 min) and recovery (7 min) times toward 5000 ppm of H_2 at 100 °C as the HEA NPs increase the number and rate of hydrogen gas molecule adsorption on the surface. DFT calculations showed that the adsorption energy of hydrogen on HEA-decorated MoS_2 is exothermic, whereas it is endothermic on pristine MoS_2, suggesting that hydrogen will adsorb more rapidly on HEA-decorated MoS_2, resulting in a shorter response time. Therefore, the synergistic effect of nanoscale junction formation between HEA and MoS_2 and the strong affinity of HEA NPs showed a 10-time increase in the response and faster response/recovery times toward hydrogen gas.

Moreover, Mondal et al. demonstrated the equiatomic TiZrVNbHf HEA NPs on MoS_2 sheets for hydrogen gas sensing.[100] Without expensive noble metals, TiZrVNbHf HEA NPs composed of relatively cheaper transition metal elements can improve hydrogen adsorption, enhancing hydrogen sensing performances. The bandgap of MoS_2 decreased from 0.11 to 0.05 eV upon TiZrVNbHf HEA NPs decoration. Additionally, the density of states (DOS) of MoS_2 with the TiZrVNbHf shifted down toward the Fermi level, around 0.51 eV, as calculated by the DFT (Figure 4f). This shift toward the Fermi level facilitates electron transfer from H_2 molecules to the TiZrVNbHf HEA NPs on MoS_2, selectively enhancing the

https://doi.org/10.1021/acssensors.4c02464
ACS Sens. 2025, 10, 33−53

sensor response to H_2. In addition, the TiZrVNbHf HEA NPs on MoS_2 generated more H_2 adsorption and dissociation, as evidenced by DFT calculation, which induced electronic charge redistribution of HEA NPs over the MoS_2.

Exsolution Catalysts. Maintaining the sensing stability against aggregation and poisoning under harsh environments is essential to provide the reliability of breath sensing results. Exsolution, a promising catalyst design, has emerged as a powerful approach for a robust catalyst synthesis process where the doped metal ions diffuse to the surface of the metal oxide sensing layer and nucleate/grow through reductive heat treatment.[50,101,102] This process results in the formation of socketed catalyst NP structures that induce reciprocal strain and smooth interfaces. The unique socketing structures of exsolved metal NPs that strongly anchor in the oxide lattice result in a robust structure with excellent thermal and chemical stability. Furthermore, the exsolution approach induces a fine-particle-size distribution based on their specific doped metal ion diffusion procedures. However, harsh reduction conditions involving balanced H_2 gas at a high temperature (>800 °C) are conducted to grow and ripen these particles, where the surface area of the support materials is often degraded. Thus, the thermally and chemically stable host oxides were needed to meet these demands.

In the early design of gas-sensing materials, exsolution catalysts have been decorated on stable supports such as perovskite oxides and yttria-stabilized zirconia (YSZ) owing to harsh exsolution process conditions. Ling Wang's group reported the development of exsolved PdO NPs on $LaFePd_{0.05}O_{3+\delta}$, Ag NPs on $AgNbO_3$, and Ag NPs on $NiFe_2Ag_{0.05}O_{4.025}$ for the impedancemetric sensors for NO_2 and NH_3 detection.[103−105] Following the exsolution process, the stable, fine, and evenly distributed heterostructure formation of the exsolved catalyst significantly enhanced catalytic activity and gas responses to such target gases.

The size, distribution, and depth of the exsolution catalysts changed catalytic properties. Kim et al. reported size and distribution-controlled Co exsolution catalysts on $La_{0.43}Ca_{0.37}Co_{0.06}Ti_{0.94}O_{3-d}$ by controlling the reduction temperature.[106] The average particle size, population, and exsolution depth varied with the reduction temperature (600, 700, and 800 °C). As the temperature increased, the driving force for exsolution was boosted, leading to an increased number of particles. However, heat-treatment at an excessive temperature induces the aggregation of these particles into larger sizes, reducing the total number of particles and catalytic activity. Considering this trade-off, the optimal Co exsolution catalyst design at 700 °C reduction temperature resulted in high sensing capability to ethanol gas with the response (R_{air}/R_{gas}) of 116.3 toward 5 ppm ethanol at 350 °C (Figure 5a). Interestingly, the numerous Co exsolution catalysts changed the majority of charge carriers from hole to electron by the formation of oxygen vacancies, which induced an improvement in sensitivity owing to conduction paths. The enhanced sensing response was attributed to the synergistic effect of the p- to n-type majority carrier transition and catalytic activity of uniformly distributed Co NPs on the host oxide.

The heat-treatment at high temperatures for extended periods and reductive gas treatment of the exsolution process confine the decorated exsolved NPs on a binary metal oxide support, which is mainly utilized for gas sensor applications. Thus, alternative internal material composition or external environment changes are needed to decorate exsolved NPs on binary oxides. Jang et al. demonstrated an ultralow temperature exsolution process in reducible WO_3 NSs.[107] Catalytic Ir doping triggered a dynamic phase transition in host WO_3, and this phase transition in WO_3 accelerated the exsolution of Ir NPs at the oxide surface (Figure 5b). The H_2S, a representative biomarker for halitosis, has a high affinity for metallic phases because of the strong chelation property with sulfur compounds. Thus, the sulfur poisoning of metal catalysts was one of the challenges for sulfur gas-contained sensing applications. The exsolved $Ir_{0.01}W_{0.99}O_3$ NSs-based sensor exhibited a significantly enhanced H_2S sensing performance compared to $Ir_{0.01}$-doped $W_{0.99}O_3$ NSs without exsolution. Specifically, exsolved-$Ir_{0.01}W_{0.99}O_3$ NSs with a reduction process at 400 °C showed the highest H_2S response (R_{air}/R_{gas} = 35 toward 5 ppm of H_2S at 375 °C), which is over 10 times higher than that of $Ir_{0.01}$-doped $W_{0.99}O_3$ NSs due to the sensitizer effect of exsolved Ir NPs.

Recently, Shin et al. demonstrated ambient-air Pt, Rh, and Ir NPs exsolution using an intensive photothermal effect on WO_3 NFs.[108] The ultrahigh photothermal effect induced by intensive irradiation can complete the exsolution process within 20 ms. With the extremely short process time, the support degradation during the exsolution process is minimized even under ambient-air conditions, making it applicable to various support materials, including binary metal oxides. This ultrafast annealing promoted mild surface reduction, leading to heterojunction formation (WO_{3-x}−WO_3), which induced large resistance changes (Figure 5c). The synergistic effects with the exsolution catalyst and formation of heterojunctions improved the gas sensing performances. As a result, a highly sensitive gas sensor for halitosis diagnosis was developed, exhibiting exceptional H_2S sensing performance (R_{air}/R_{gas} > 800 toward 1 ppm of H_2S at 80% RH and 350 °C). According to previous studies, exsolved NPs exhibited excellent resistance to sintering and coking due to their socketed geometry. Similarly, exsolution catalysts loaded on WO_3 maintained stable H_2S sensing characteristics over 80 repeated sensing cycles. The stable socketed exsolution catalyst allowed the exsolved NPs to remain on the WO_3 after cyclic sensing tests, even at an elevated temperature of 350 °C.

With the strategies for moderating the harsh exsolution condition, the range of material design of catalysts and supports has been expanded. However, it is still challenging to precisely control the synthetic factors such as composition, size, and distribution of exsolution catalysts on binary metal oxides in such an exsolution environment. To address these challenges, a new strategy has been proposed to synthesize the desired exsolution catalyst on a stable support and then integrate them with a binary metal oxide sensing material in a hybrid structure (Figure 5d).[109] $La_{0.6}Ca_{0.4}Fe_{0.95}Co_{0.05-x}Ni_xO_{3-\delta}$ (LCF) NFs were stable supports for the exsolution process. The size of exsolved catalysts with various elements (Co, Ni, CoNi, and CoNiFe) was controlled by the reduction temperature (600, 700, and 800 °C in 4% H_2). These controlled exsolved catalysts were mixed with a Sn precursor and PVP polymer, and the hybrid NFs were synthesized via electrospinning. Subsequent calcination led to polymer decomposition, Sn precursor oxidation, and the formation of exsolved NPs on LCF@SnO_2 NFs. These heterointerfaces, 1) exsolved NPs-LCF, 2) heterojunction of LCF-SnO_2 NFs, and 3) the sensitizer effect of the exsolution catalyst, enabled the development of a highly sensitive and durable sulfuric compound gas sensor with the response (R_{air}/R_{gas}) over 148

https://doi.org/10.1021/acssensors.4c02464
ACS Sens. 2025, 10, 33−53

toward 5 ppm dimethylsulfide (DMS) at 90% RH for CoNiFe exsolved NPs on LCF@SnO_2. This strategy also allows facile selectivity tuning by adjusting the exsolution catalyst composition. For example, a high gas response of 30 was achieved toward 5 ppm of methyl mercaptan (CH_3SH) at 90% RH using Co NPs on $La_{0.6}Sr_{0.4}Mn_{0.85}Co_{0.15}O_{3-\delta}$@$SnO_2$ NFs.

Catalytic Filter. In the earlier sections, we introduced the achievements that improved gas sensing performances using catalyst decoration on sensing materials. Here, we present a different approach that utilizes a catalyst for gas decomposition in ambient air entering the sensor. While previous catalytic strategies focus on modulating the surface chemical activity toward specific gases, the catalytic filter strategy aims to improve gas selectivity by removing interfering gas components. This strategy can be categorized into two main approaches: 1) inserting a catalytic bed upstream of the gas sensor to remove interfering gases and 2) depositing a catalyst membrane directly onto the sensing material to achieve in situ interfering gas removal. The catalytic bed method embeds the filter in front of the sensor devices, removing interfering gases from the external atmosphere and injecting pretreated air at the sensing materials.[110−113] Guntner et al. developed a gas sensor integrated with a ZnO-based catalytic bed for acetone detection with selective removal of ethanol from exhaled breath (Figure 5e).[58] The ZnO catalytic bed can completely decompose ethanol at 200 °C and acetone at 300 °C, allowing for selective removal of ethanol by operating at an intermediate temperature (Figure 5f). This approach successfully improved the accuracy of acetone detection even in exhaled breath samples following alcohol consumption (Figure 5g). Furthermore, the gas selectivity can be enhanced by modifying the catalyst within the catalytic bed. Weber et al. demonstrated that incorporating Pt-loaded Al_2O_3 NPs into the catalytic bed effectively removed various interfering gases (isoprene, ethanol, H_2, CO, and NH_3), thereby improving selectivity toward acetone.[114] By exploiting the temperature-dependent decomposition characteristics of different gases, they achieved selective acetone detection at 100 °C. Using a more efficient catalyst such as Pt−Al_2O_3 allowed for the decomposition of other gases at lower temperatures compared to the above references using ZnO particles, offering an energy efficiency with low power consumption. This Pt−Al_2O_3 catalytic bed showed high gas selectivity for acetone, even in high-humidity conditions relevant to breath analysis, confirming its capability to selectively retain acetone in mixed gas environments.

By effectively removing interference gases, catalytic beds improve the reliability of sensor results, particularly for VOCs, which exhibit similar chemical activity on the surfaces of sensing materials and are challenging to distinguish. However, incorporating a separate catalytic bed into the sensor device introduces an additional fabrication process, leading to a loss of gas flow with a lowered actual gas concentration. To address these limitations, the second approach utilizes a catalytic membrane deposited directly onto the sensing material with micrometer thickness.[115−117] Moon et al. enhanced gas selectivity for breath analysis by depositing a Ru-TiO_2 catalyst membrane on a SnO_2 sensing material (Figure 5h).[118] Although BTX (benzene, toluene, and xylene) gases are biomarkers for different diseases, they are challenging to differentiate using conventional gas sensors due to their similar molecular structures. In that study, a catalytic overlayer was used to differentiate between these gases based on the catalytic activity of Ru. A catalytic overlayer deposited directly onto the sensor facilitates the diffusion of partially decomposed intermediates into the sensing layer during gas decomposition (Figure 5i). These highly reactive intermediates enhance the gas response, known as the gas reforming effect. This effect enables the sensor device to distinguish between gases by modulating the gas response based on decomposition rates. In this case, the more reactive xylene gas readily decomposes at the catalytic overlayer, while the less reactive benzene exhibits a slower decomposition process. For pure SnO_2, higher gas responses toward xylene were observed as a result of its higher reactivity near the surface of the gas sensing layer. With the small amount (0.5 wt %) of Rh-loaded catalytic overlayer, the overall gas responses to target gases were increased due to the gas reforming effect. As the Ru catalyst loading increases, highly reactive gases undergo complete decomposition into less reactive components while the reforming effect on relatively stable gases persists. Consequently, the order of gas response changes from xylene to toluene to benzene as the Rh content increases from 0.5 wt % (0.5Rh-TiO_2/SnO_2) to 1 wt % (1Rh-TiO_2/SnO_2) and 2 wt % (2Rh-TiO_2/SnO_2) (Figure 5j). This approach allows for tuning the gas selectivity and improving the benzene selectivity. The catalytic filter strategy can be effectively integrated into existing high-performance gas sensor technologies, significantly enhancing the gas selectivity for detecting specific biomarkers in interfering mixture gases. It is expected to be crucial in implementing target-specific breath analyzers for detecting specific biomarkers.

NOVEL APPROACHES ON CATALYST DESIGN AND INTEGRATION INTO BREATH SENSORS

Emerging thermal treatment methods, i.e., thermal-shock annealing, are being explored to incorporate novel catalysts that are challenging to use in gas sensors, including carbothermal and flash-thermal shocks, owing to their unique processing advantages such as overcoming the thermodynamic equilibrium and minimizing thermal degradation of support oxides. In addition, research in gas sensor development increasingly utilizes computational approaches such as artificial intelligence (AI) and machine learning to predict highly active catalyst compositions and systems. In this section, we introduced computational-calculation-based investigation of optimal alloy compositions and combinations for specific gases. Such methods have led to the discovery of new catalysts with high reactivity toward the target gases. Furthermore, by integrating these cutting-edge sensing materials into arrays and employing AI-based predictions, the accuracy of gas sensing is significantly enhanced, potentially rationalizing noninvasive diagnosis by breath analysis.

Emerging Catalyst Design by Thermal-Shock Synthesis. In addition to synthesizing the aforementioned novel catalysts, finer control over their size and composition is crucial for maximizing catalytic activity. Thermal-shock synthesis, with its rapid ramping and cooling rates, enables such precise control in catalyst synthesis. Furthermore, this method offers several advantages, including low energy consumption, a relatively simple working principle, short processing times, and the ability to produce nonequilibrium or metastable nanomaterials such as SAC catalyst, HEA catalyst, and exsolved catalyst.[119−124] To induce thermal-shock in support materials, powerful external force fields are required. Binary metal oxides, such as SnO_2, WO_3, and ZnO, are the most commonly used catalyst support materials in gas sensors. A method involving intensive light irradiation has been proposed

https://doi.org/10.1021/acssensors.4c02464
ACS Sens. 2025, 10, 33−53

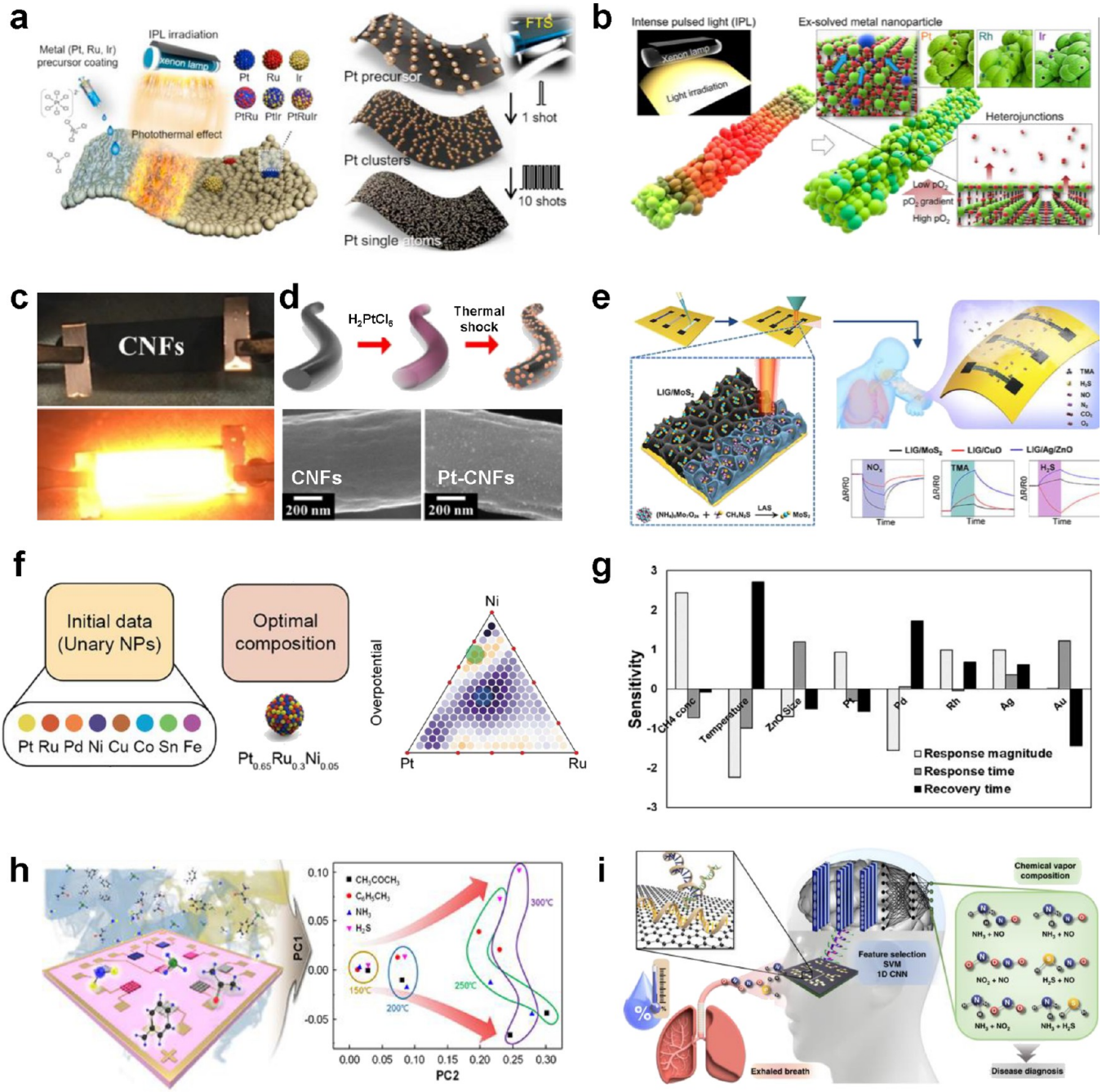

Figure 6. (a) Schematic illustrations of flash-thermal shock-based synthesis of alloy and single-atom catalysts. Reproduced with permission from ref 126. Copyright 2022 Cell press. (b) Schematics illustration of flash-thermal shock synthesis of exsolution catalysts and proposed mechanism for the formation of exsolved metal NPs. Reproduced with permission from ref 108. Copyright 2022 American Chemical Society. (c) Camera images of carbon thermal-shock on CNFs and (d) Schematic illustrations of carbon thermal shock with SEM images of CNF and Pt-CNF. Reproduced with permission from ref 127. Copyright 2022 Elsevier. (e) Schematic illustrations of laser-driven thermal-shock synthesis of various sensing materials such as MoS_2, CuO, and Ag-loaded ZnO. Reproduced with permission from ref 128. Copyright 2023 Elsevier. (f) Schematic illustration of the active learning-based catalyst design. Reproduced with permission from ref 131. Copyright 2022 Wiley-VCH GmbH. (g) Sensitivity analysis of the independent variables and Pareto solutions of the responses. Reproduced with permission from ref 132. Copyright 2019 Elsevier. (h) Schematic illustration of the 3 × 3 gas sensor array and PCA result of multiple gases based on gas responses at different operating temperatures. Reproduced with permission from ref 147. Copyright 2021 Royal Society of Chemistry. (i) Schematic diagram of exhaled breath analysis using DNA functionalized graphene gas sensor array with an AI-assisted data analysis technique. Reproduced with permission from ref 155. Copyright 2023 Springer Nature.

to synthesize catalysts on these metal oxides through thermal shock, using the photothermal effect. This photothermal-based thermal shock exposes materials to specific wavelengths or bands, leading to light-to-heat conversion processes.[125] Kim et al. reported that the photothermal effect on metal oxides can be optimized by considering crystalline size, defects, bandgap transitions, thermal conductivity, and porosity (Figure 6a).[126] By enhancing these properties, they synthesized SnO_2 NSs with high photothermal efficiency, including temperature exceeding 1800 °C within 20 ms, ramping and cooling rates

https://doi.org/10.1021/acssensors.4c02464
ACS Sens. 2025, 10, 33−53

of 1.4×10^5 and 4.6×10^4 °C/sec, respectively. This approach was used to fabricate binary, ternary alloy catalysts, including PtRu, PtIr, and PtRuIr, as well as Pt single-atom catalysts on SnO_2 NSs, which were applied for VSC sensing, which related to intraoral or extra-oral diseases from exhaled breath of patients. Additionally, Shin et al. reported the exsolution of Pt, Rh, and Ir catalysts on WO_3 NFs using an intensive photothermal effect at ambient-air conditions (Figure 6b).[108] As previously mentioned, the exsolution process has limitations when applied to binary metal oxides due to harsh reductive treatments. To overcome these challenges, the intensive photothermal effect was employed to create a mild reductive environment on the surface within milliseconds, enabling the exsolution of catalysts. This approach to catalyst design using the photothermal effect enables the attachment of small and uniform nanocatalysts to metal oxide surfaces. The photothermal effect of the support material makes it easier to anchor the catalysts, which is particularly advantageous for designing catalysts based on gas detection mechanisms that involve reactions of surface with gases.

The additional thermal-shock synthesis is based on joule heating derived from an electric current flowing through a resistive element. Most metal oxides have a high resistance to achieve the high temperatures required for thermal shock. To address this issue, Chae et al. demonstrated a method where thermal-shock-stabilized Pt NPs were first decorated on carbon nanofibers (CNFs) (Figure 6c,d).[127] Afterward, a sputtering process followed by an oxidative heat treatment decomposed the carbon, resulting in the synthesis of SnO_2 hemitubes. Although this method has limitations in directly functionalizing catalysts on metal oxide supports, it offers the advantage of synthesizing various catalysts through joule heating and subsequently anchoring them to different metal oxides, thereby enabling functionalization across a range of oxide materials. Laser-driven thermal-shock processes are generally faster and have higher energy than those driven by light or joule heating, making it easier to overcome thermodynamic limitations and synthesize metastable nanomaterials. Zhao et al. demonstrated the versatility of laser-assisted synthesis for gas sensing materials, successfully synthesizing a range of catalysts, including transition metal dichalcogenides, metal oxides, noble metal-doped metal oxides, and composite metal oxides on graphene for the detection of multiple gas analytes such as NO_2, trimethylamine (TMA), and H_2S, including MoS_2, CuO, and Ag/ZnO with low detection limit, 2.7, 9.8, and 5.6 ppb, respectively (Figure 6e).[128] In summary, these novel catalysts are being synthesized through various thermal-shock methods. Research in thermal shock-based catalyst design is progressing owing to their exceptional advantages for overcoming the thermodynamic equilibrium, and it is expected to be increasingly applied to the design of gas sensor catalysts, helping to overcome previous challenges associated with conventional catalysts in gas sensing applications.

Computational Calculations for Outperforming Gas Sensors. Optimizing the catalytic properties of complex catalysts through the rational design of synthetic factors is crucial to developing high-performance gas sensors. To predict the composition and systems of highly active catalysts, computational approaches, including AI and machine learning, have been employed to design novel catalysts. However, these methods are often limited by exhaustive data requirements and high costs associated with experimental trials. Therefore, active learning can facilitate the development of more effective models (Figure 6f).[129−131] With a comprehensive understanding of unary catalysts with initial measurement data, the properties of complex compositional catalysts can be predicted by constructing an appropriate model. This approach is particularly crucial in designing catalysts for gas sensors, where it has not been extensively explored and, thus, requires effective modeling strategies. Ghosal et al. demonstrated a data-driven approach for designing ternary alloy catalysts for methane sensors.[132] These three parameters are critical for sensing performances, but optimizing them simultaneously can be challenging due to their often trade-off behaviors (Figure 6g). To address this issue, multiobjective optimization using genetic algorithms plays a crucial role and has been successfully employed to design alloys that balance these conflicting objectives. The Pareto solution is a concept for finding optimization of specific properties on trade-off behaviors. Pareto fronts generated as the result of the optimization process, which consist of nondominated optimal solutions, were used to identify trends in combinations and compositions, ultimately guiding the design of the alloy. Therefore, Pt−Pd−Ag, Pt−Ag−Au, and Pd−Rh−Ag outperformed other possible combinations based on Pareto solutions, with Pt−Pd−Ag identified as the most promising for methane sensors. This finding provides valuable guidance for future experimental trials.

Integration into Sensor Array for Breath Analysis with AI technique. Various catalysts using novel synthetic methods introduced in this review have significantly enhanced the performance of chemiresistive gas sensors, thereby enabling their application in breath analysis. With these advances in gas sensors, intensive research is underway to encourage laboratory-scale achievements into practical, real-world applications. Given the complex composition of exhaled breath, developing reliable diagnostic tools is crucial for successfully implementing breath analysis. Employing sensor arrays, characterized as "electrical nose" (e-nose) rather than individual sensors is advantageous to enhance sensing reliability in breath analysis.[133−136] The overall system can more accurately detect and analyze gas mixtures by combining multiple sensors with different gas selectivity. In practice, commercial gas sensors often employ arrays of different sensors to mitigate the effects of environmental variables.[137−139] Recent research trends have emphasized the utilization of AI to analyze gas response data and improve system reliability.[140−142]

AI algorithms construct databases based on gas response patterns, gas types, concentrations, humidity, and temperature to accurately identify the target gases within complex gas mixtures. Previous studies using sensor arrays have shown that gas species can be distinguished using basic data analysis methods such as principal component analysis (PCA) and linear discriminant analysis (LDA).[10,143−146] Lee et al. fabricated a 3 × 3 gas sensor array with 3 different types of metal oxides, WO_3, SnO_2, and NiO (Figure 6h).[147] Three metal oxides were constructed as thin films, nanodomes, and Au NPs decorated nanodomes. These nanodome structures enhance the overall gas response but exhibit similar gas selectivity. After Au NP decoration, Au NPs selectively enhance gas responses, resulting in gas selectivity changes. With the gas selectivity differences, this sensor array can distinguish four target gases such as C_3H_6O, C_7H_8, NH_3, and H_2S, using the PCA method. Freddi et al. fabricated a gas sensor array based on different types of CNT by changing the

https://doi.org/10.1021/acssensors.4c02464
ACS Sens. 2025, 10, 33−53

Table 1. Summary of Emerging Catalyst-loaded Chemiresistive Gas Sensors for Breath Analysis

Catalysts	Catalyst elements	Sensing layers	Target gas	Response ($\|R_{air}/R_{gas}\|$)	Humidity (R.H. %)	Related disease	ref.
Doping catalyst	Co, N	WS_2@carbon nanocages	NO_2	48.2% at 5 ppm	dry	Lung cancer	63
	Sb	SnO_2@ZnO	C_3H_6O	12.8 at 5 ppm	90	Diabetes	64
	PEI	PNDIT2	NO_2	264% at 5 ppm	dry	Lung cancer	65
	Al	SnO_2	C_2H_6O	14 at 100 ppm	dry	Liver dysfunction	69
	Eu	SnO_2	C_3H_6O	32.3 at 100 ppm	60	Diabetes	70
	B	rGO	NO_2	~ 4% at 5 ppm	80	Lung cancer	82
	Co	CeO_2@SnO_2	C_5H_8	120.38 at 5 ppm	75	Cholesterol metabolism	159
Single-atom catalyst	Pt	SnO_2	HCHO	33.9 at 5 ppm	dry	Cancers, Lungs	76
	Pt	SnO_2	C_3H_6O	~ 38 at 5 ppm	95	Diabetes	77
	Ni	N doped rGO	NO_2	~ 1.9% at 1 ppm	dry	Lung cancer	82
	Co	N-doped carbon support	NH_3	7.6% at 5 ppm	dry	Kidney dysfunction	160
	Pt	Ag-doped $LaFeO_3$@ZnO	CH_3OH	453.05 at 5 ppm	dry	Alcohol metabolism	161
Bimetallic alloy catalyst	PtPd	WO_3	C_3H_6O	97.5 at 1 ppm	90	Diabetes	42
	PtRh	WO_3	C_3H_6O	104 at 1 ppm	90	Diabetes	42
	AuPt	ZnO	H_2S	17.7 at 20 ppm	dry	Halitosis	55
	PdAu	ZnO	H_2	169 at 100 ppm	dry	Gastrointestinal disorders	88
	PdAu	SnO_2	H_2	46.4 at 100 ppm	dry	Gastrointestinal disorders	89
	PdAu	ZnO	H_2	80 at 100 ppm	dry	Gastrointestinal disorders	90
	AgAu	ZnO	C_2H_6O	1755 at 100 ppm	dry	Liver dysfunction	91
	PtRu	$Cu_3(HHTP)_2$	NO_2	~ 40% at 3 ppm	80	Lung cancer	94
	PtIr	SnO_2	H_2S	3165 at 1 ppm	90	Halitosis	126
	PtRuIr	SnO_2	C_2H_6S	6089 at 1 ppm	90	Halitosis	126
	PdRu	SnO_2	TEA	256 at 100 ppm	dry	Liver dysfunction	162
High entropy alloy catalyst	AgAuCuPdPt	MoS_2	H_2	~ 30% at 1000 ppm	dry	Gastrointestinal disorders	99
	TiZrVNbHf	MoS_2	H_2	~ 50% at 100 ppm	dry	Gastrointestinal disorders	100
Exsolution catalyst	Co	$La_{0.43}Ca_{0.37}Co_{0.06}Ti_{0.94}O_{3-x}$	C_2H_6O	116.3 at 5 ppm	dry	Liver dysfunction	106
	Ir	WO_3	H_2S	35 at 5 ppm	dry	Halitosis	107
	Pt	WO_3	H_2S	~ 850 at 1 ppm	90	Halitosis	108
	CoNiFe	SnO_2	C_2H_6S	148 at 5 ppm	90	Halitosis	109
Catalytic filter	Pt−Al_2O_3	Si-doped WO_3	C_3H_6O	5.4 at 1 ppm	90	Diabetes	114
	Pt-ZIF8	ZnO	H_2S	~ 58 at 5.5 ppm	75	Halitosis	163

surface properties.[148] They decorated different types of organic molecules on the surface of the CNT to change the gas selectivity. A total of 8 different gas sensors were integrated into a single sensor device and measured the gas responses to various kinds of gas species, which can be included and presented in the exhaled breath of chronic obstructive pulmonary disease patients. With the gas response measurement data, the breath print of real patients was obtained by PCA analysis and distinguished the breath of patients. In addition, Duan et al. prepared a W-CeO_2 nanosphere to detect H_2S gas in exhaled breath for halitosis diagnosis.[149] 7% of W doping in the CeO_2 nanosphere can improve gas response to H_2S. The sensor array was composed of different doping concentrations of W in CeO_2. To verify the H_2S detection capability of the sensor array, simulated exhaled breath was prepared by introducing 100 ppb of H_2S or 200 ppb of ethanol to normal human exhaled breath. This sensor array can distinguish each exhaled breath by the LDA algorithm. These PCA and LDA methods effectively analyze sensing data from gas sensors, demonstrating the feasibility of diagnosis of diseases from exhaled breath.

Consequently, with the rapid advances in AI algorithms for data analysis, such as machine learning and deep learning algorithms, research is increasingly focused on improving diagnostic accuracy with AI-based analytical techniques.[150−154] Hwang et al. fabricated a DNA-functionalized graphene gas sensor array to discriminate three biomarkers, i.e., H_2S, NO, and NH_3, using an AI-based algorithm (Figure 6i).[155] To analyze the gas sensing data, they adopted two algorithms: machine learning-based support vector machine (SVM) classification and deep learning-based 1D convolutional neural network (CNN) method. The SVM method classifies the data by finding the optimal hyper-line or plane that maximizes the distance with each class of data.[156,157] To employ this SVM method for analyzing the gas types, features such as the magnitude, derivative, difference, time, and area of gas responses are selected. The SVM-based classification exhibits almost 98% accuracy for mixed gas components. Next, the deep learning-based 1D CNN algorithm, inspired by the human visual cortex, is a neural network designed to process sequential data by applying convolutional filters along one dimension to capture local patterns, often used in signal processing.[158] This 1D CNN algorithm performed perfect gas classification results for mixed gas combinations even under humid conditions, offering a more automated classification process without arbitrary feature selection. These AI-based gas discrimination methods can effectively and accurately analyze target gases in mixed gas states. Integrating AI-based analysis

https://doi.org/10.1021/acssensors.4c02464
ACS Sens. 2025, 10, 33−53

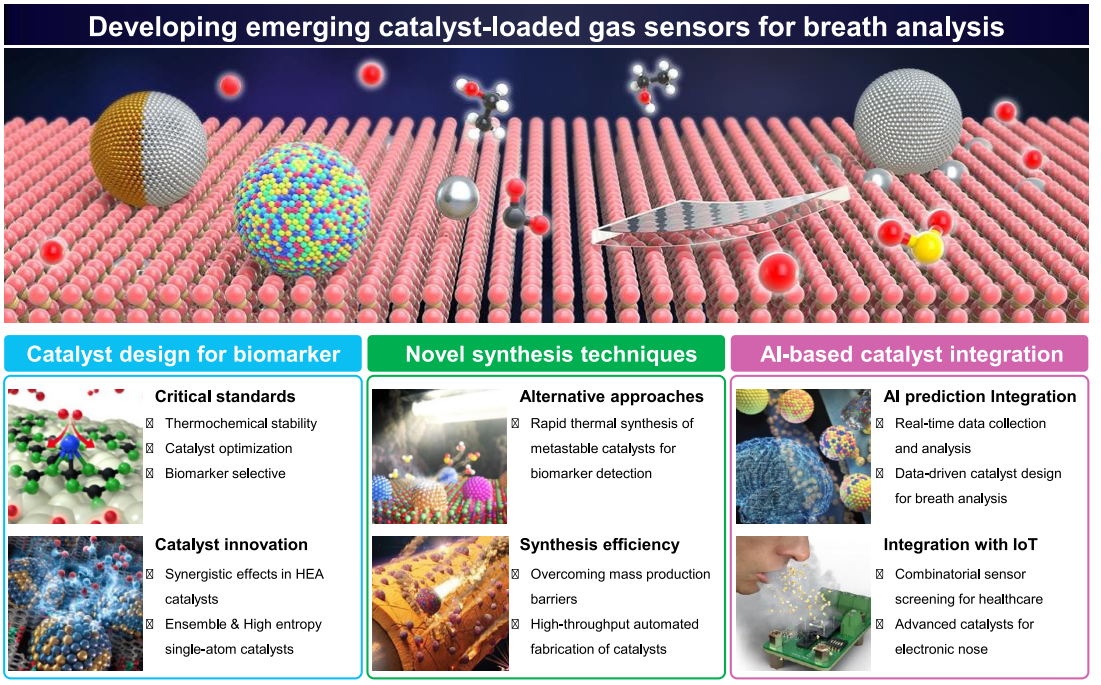

Figure 7. Future perspectives and challenges for innovating gas sensors by catalyst technologies for breath analysis. Reproduced with permission from ref 76. Copyright 2020 American Chemical Society. Reproduced with permission from ref 94. Copyright 2021 Wiley-VCH GmbH. Reproduced with permission from ref 108. Copyright 2022 American Chemical Society. Reproduced with permission from ref 164. Copyright 2023 American Chemical Society. Reproduced with permission from ref 130. Copyright 2022 Wiley-VCH GmbH. Reproduced with permission from ref 165. Copyright 2021 American Chemical Society.

techniques with sensor arrays drives advancements in gas sensor development for diagnostic applications. To increase the efficiency and accuracy of AI-based analysis, the performance of individual gas sensors within the array and the design of the sensor array are important. In particular, robust gas selectivity of the constituent sensors is pivotal for ensuring reliable diagnosis of diseases. Consequently, the development of high-performance catalysts is essential for advancing future gas sensor technologies.

CONCLUSIONS AND PERSPECTIVES

This Account presents the recent advances in catalysts and their roles in enhancing the sensing performance of chemiresistive gas sensors for applications in breath analysis (Table 1). Promising catalyst design and synthesis techniques have been developed for innovative gas sensors, demonstrating the feasibility of disease diagnosis and health monitoring by breath analysis. SACs and heteroatom doping utilize singular atoms as catalysts, boosting surface activity and catalytic efficiency. Bimetallic alloy catalysts improve catalytic performance by combining metals to leverage synergistic effects. With its complex composition of multiple principal elements, HEA offers unique catalytic properties, lowering reaction barriers for surface chemical reactions. By embedding metal NPs with a socketed structure within an oxide matrix, exsolution catalysts provide improved stability and prolonged catalytic performance, pursuing challenges for reliable sensing properties toward sulfuric gas compounds. The catalytic filter strategy enhances gas sensor selectivity by pretreating ambient air with catalysts through a catalytic bed or a membrane applied directly onto the sensing material to remove interfering gases.

Regarding new catalyst designs and synthesis, computational calculations and machine learning enhance gas sensor design by optimizing performance and catalyst attributes, while advanced synthesis methods ensure precise control over catalyst properties. As an example of a catalyst synthesis method, the thermal shock technique is highlighted owing to its unique ability to produce nonequilibrium or metastable nanomaterials by exposing extensive thermal energy within milliseconds, resulting in unprecedented catalytic activities. Classification and identification of breath biomarkers can be accomplished by assembling diverse catalyst-decorated sensing materials into a sensor array. In addition, integrating sensor arrays with AI-based analysis improves reliability and selectivity, advancing gas sensor technology for disease diagnosis and healthcare applications by exhaled breath analysis.

The recent advances in emerging catalysts discussed in this review highlight the potential of breath analysis for disease diagnosis. Establishing a reliable diagnosis is imperative to ensuring the clinical relevance of breath analysis. Consequently, further advancements in gas sensor technology for breath analysis are necessary from diverse perspectives (Figure 7). Regarding catalyst design, it is essential to prioritize catalytic capability for gas sensitivity and selectivity. Moreover, forthcoming catalysts should consider (i) thermochemical stability for reliable gas detection under harsh measurement conditions such as highly humid conditions, (ii) catalyst loading optimization for maximizing active sites, and (iii) material design for specific biomarkers with one-to-one correspondence, incorporating innovative atomic-scale engineering strategies. To address these critical criteria, advancements in catalyst synthesis are crucial for fabricating rationally designed catalysts that enable precise control over catalysts at the atomic level. In conjunction with advancements in gas sensor technology, AI-based data analysis techniques can guide

https://doi.org/10.1021/acssensors.4c02464
ACS Sens. 2025, 10, 33−53

the design of catalyst materials and sensor devices. Additionally, integrating advanced catalysts into sensor array platforms without compromising performance or adding excessive complexity is difficult, and scaling laboratory techniques to the commercial production domain while maintaining high performance is crucial. Following the collaborative progress, emerging catalysts and advanced sensing layers hold great promise for the future of breath analysis and diagnosis.

AUTHOR INFORMATION

Corresponding Authors

Seon-Jin Choi − *Division of Materials of Science and Engineering, Hanyang University, Seoul 04763, Republic of Korea;* orcid.org/0000-0001-8567-0668; Email: sjchoi27@hanyang.ac.kr

Il-Doo Kim − *Department of Materials Science and Engineering, Korea Advanced Institute of Science and Technology (KAIST), Daejeon 34141, Republic of Korea;* orcid.org/0000-0002-9970-2218; Email: idkim@kaist.ac.kr

Authors

Jong Won Baek − *Department of Materials Science and Engineering, Korea Advanced Institute of Science and Technology (KAIST), Daejeon 34141, Republic of Korea*

Euichul Shin − *Department of Materials Science and Engineering, Korea Advanced Institute of Science and Technology (KAIST), Daejeon 34141, Republic of Korea*

Jinho Lee − *Department of Materials Science and Engineering, Korea Advanced Institute of Science and Technology (KAIST), Daejeon 34141, Republic of Korea*

Dong-Ha Kim − *Department of Materials Science & Chemical Engineering, Hanyang University-ERICA, Ansan, Gyeonggi-do 15588, Republic of Korea*

Complete contact information is available at: https://pubs.acs.org/10.1021/acssensors.4c02464

Author Contributions

■J.W.B., E.S., and J.L. contributed equally to this work. All the authors take full responsibility for the content of this review and approve its submission.

Notes

The authors declare no competing financial interest.

ACKNOWLEDGMENTS

This work was supported by the National Research Foundation of Korea (NRF) grant funded by the Korea government (MSIT) (No. RS-2023-00236572 and RS-2024-00407282). This work was supported by the National Research Foundation of Korea grant funded by the Korea government, Ministry of Science and ICT (Development of Nanofiber Yarn Based Compound Sensor as a Comprehensive Wearable Healthcare Solution) (Grant No. RS-2024-00357296).

VOCABULARY

Volatile Organic Compounds (VOCs), are organic chemicals that easily evaporate at room temperature, contributing to air pollution and potentially causing adverse health effects; **A gas sensor**, is a device that detects the presence and concentration of gases in the environment by converting chemical information into an electrical signal; **Doping**, is the intentional introduction of impurities into a material to modify its electrical, optical, or structural properties. A single atom refers to an individual atom, often used in catalysis, where it is isolated and stabilized on a support material to maximize its catalytic efficiency; **Exsolution**, is a process in which a solid solution phase separates into distinct phases, often leading to the formation of nanoparticles or secondary phases within a host material; **A bimetallic alloy**, is a material composed of two different metals that are combined to enhance properties such as strength, corrosion resistance, or catalytic activity; **A high-entropy alloy**, is a type of alloy composed of five or more principal elements in near-equal atomic percentages, leading to a material with unique properties due to its high configurational entropy; **A catalytic filter**, is a filtration device that incorporates a catalyst to simultaneously remove particulate matter and catalyze chemical reactions

REFERENCES

(1) Buszewski, B.; Kęsy, M.; Ligor, T.; Amann, A. Human exhaled air analytics: biomarkers of diseases. *Biomed. Chromatogr.* **2007**, *21* (6), 553−566.

(2) Das, S.; Pal, M. Non-invasive monitoring of human health by exhaled breath analysis: A comprehensive review. *J. Electrochem. Soc.* **2020**, *167* (3), No. 037562.

(3) Mayer, M.; Baeumner, A. J. A megatrend challenging analytical chemistry: biosensor and chemosensor concepts ready for the internet of things. *Chem. Rev.* **2019**, *119* (13), 7996−8027.

(4) Tangerman, A. Measurement and biological significance of the volatile sulfur compounds hydrogen sulfide, methanethiol and dimethyl sulfide in various biological matrices. *J. Chromatogr. B* **2009**, *877* (28), 3366−3377.

(5) Kharitonov, S.; Yates, D.; Robbins, R.; Barnes, P.; Logan-Sinclair, R.; Shinebourne, E. Increased nitric oxide in exhaled air of asthmatic patients. *Lancet* **1994**, *343* (8890), 133−135.

(6) Righettoni, M.; Tricoli, A. Toward portable breath acetone analysis for diabetes detection. *J. Breath Res.* **2011**, *5* (3), No. 037109.

(7) Španěl, P.; Davies, S.; Smith, D. Quantification of breath isoprene using the selected ion flow tube mass spectrometric analytical method. *Rapid Commun. Mass Spectrom.* **1999**, *13* (17), 1733−1738.

(8) Hori, A.; Suijo, K.; Kondo, T.; Hotta, N. Breath isoprene excretion during rest and low-intensity cycling exercise is associated with skeletal muscle mass in healthy human subjects. *J. Breath Res.* **2021**, *15* (1), No. 016009.

(9) Hakim, M.; Broza, Y. Y.; Barash, O.; Peled, N.; Phillips, M.; Amann, A.; Haick, H. Volatile organic compounds of lung cancer and possible biochemical pathways. *Chem. Rev.* **2012**, *112* (11), 5949−5966.

(10) Cho, H.-J.; Kim, S.-J.; Choi, S.-J.; Jang, J.-S.; Kim, I.-D. Facile synthetic method of catalyst-loaded ZnO nanofibers composite sensor arrays using bio-inspired protein cages for pattern recognition of exhaled breath. *Sens. Actuators, B* **2017**, *243*, 166−175.

(11) Park, S.; Lim, Y.; Oh, D.; Ahn, J.; Park, C.; Kim, M.; Jung, W.; Kim, J.; Kim, I.-D. Steering selectivity in the detection of exhaled biomarkers over oxide nanofibers dispersed with noble metals. *J. Mater. Chem. A* **2023**, *11* (7), 3535−3545.

(12) Cho, D.; Suh, J. M.; Nam, S.H.; Park, S. Y.; Park, M.; Lee, T. H.; Choi, K. S.; Lee, J.; Ahn, C.; Jang, H. W.; Shim, Y.S.; Jeon, S. Optically activated 3D thin-shell TiO_2 for super-sensitive chemoresistive responses: toward visible light activation. *Adv. Sci.* **2021**, *8* (3), 2001883.

(13) Choi, S.-J.; Kim, I.-D.; Park, H. J. 2D layered Mn and Ru oxide nanosheets for real-time breath humidity monitoring. *Appl. Surf. Sci.* **2022**, *573*, No. 151481.

(14) Choi, S.-J.; Fuchs, F.; Demadrille, R.; Grévin, B.; Jang, B.-H.; Lee, S.-J.; Lee, J.-H.; Tuller, H. L.; Kim, I.-D. Fast responding exhaled-breath sensors using WO_3 hemitubes functionalized by graphene-

based electronic sensitizers for diagnosis of diseases. *ACS Appl. Mater. Interfaces* **2014**, *6* (12), 9061−9070.
(15) Choi, S.-J.; Ku, K. H.; Kim, B. J.; Kim, I.-D. Novel templating route using Pt infiltrated block copolymer microparticles for catalytic Pt functionalized macroporous WO_3 nanofibers and its application in breath pattern recognition. *ACS Sens.* **2016**, *1* (9), 1124−1131.
(16) Park, S.; Kim, M.; Lim, Y.; Oh, D.; Ahn, J.; Park, C.; Woo, S.; Jung, W.; Kim, J.; Kim, I.D. Dual-Photosensitizer Synergy Empowers Ambient Light Photoactivation of Indium Oxide for High-Performance NO_2 Sensing. *Adv. Mater.* **2024**, *36* (24), 2313731.
(17) Shin, J.; Choi, S. J.; Lee, I.; Youn, D. Y.; Park, C. O.; Lee, J. H.; Tuller, H. L.; Kim, I.-D. Thin-wall assembled SnO_2 fibers functionalized by catalytic Pt nanoparticles and their superior exhaled-breath-sensing properties for the diagnosis of diabetes. *Adv. Funct. Mater.* **2013**, *23* (19), 2357−2367.
(18) Baek, J. W.; Kim, Y. H.; Ahn, J.; Kim, D.-H.; Shin, H.; Ko, J.; Park, S.; Park, C.; Shin, E.; Jang, J.-S.; Kim, I.-D. Galvanic replacement reaction in perovskite oxide for superior chemiresistors. *J. Mater. Chem. A* **2022**, *10* (43), 23282−23293.
(19) Song, L.; Ahn, J.; Xu, L.; Baek, J. W.; Shin, E.; Kim, I.-D. Facile synthesis of $Co_3O_4/CoMoO_4$ heterostructure nanosheets for enhanced acetone detection. *ACS Sens.* **2022**, *7* (11), 3540−3550.
(20) Kim, S.-J.; Choi, S.-J.; Jang, J.-S.; Kim, N.-H.; Hakim, M.; Tuller, H. L.; Kim, I.-D. Mesoporous WO_3 nanofibers with protein-templated nanoscale catalysts for detection of trace biomarkers in exhaled breath. *ACS Nano* **2016**, *10* (6), 5891−5899.
(21) Song, Y. G.; Park, J. Y.; Suh, J. M.; Shim, Y.-S.; Yi, S. Y.; Jang, H. W.; Kim, S.; Yuk, J. M.; Ju, B.-K.; Kang, C.-Y. Heterojunction based on Rh-decorated WO_3 nanorods for morphological change and gas sensor application using the transition effect. *Chem. Mater.* **2019**, *31* (1), 207−215.
(22) Lee, S.; Choi, S.; Park, S. H.; Cho, S. H.; Sohn, W.; Eom, T. H.; Kim, Y.; Jang, H. W. Synthesis-in-place hydrothermal growth of hematite nanorods on patterned substrate for highly sensitive and rapid acetone detection. *Sens. Actuators, B* **2023**, *395*, No. 134519.
(23) Cho, S. H.; Choi, M.-J.; Koo, B.; Kim, J.; Lee, T. H.; Suh, J. M.; Eom, T. H.; Park, S. Y.; Kim, T.; Jung, W.; Jang, H. W. Rapid and ultrahighly sensitive ethanol sensing in p-type $SrTi_{1-x}Fe_xO_3$. *Sens. Actuators, B* **2024**, *403*, No. 135137.
(24) Gu, D.; Liu, W.; Wang, J.; Yu, J.; Zhang, J.; Huang, B.; Rumyantseva, M. N.; Li, X. Au functionalized SnS_2 nanosheets based chemiresistive NO_2 sensors. *Chemosensors* **2022**, *10* (5), 165.
(25) Mishra, R. K.; Choi, G. J.; Mishra, Y. K.; Kaushik, A.; Sohn, Y.; Lee, S. H.; Gwag, J. S. A highly stable, selective, and high-performance VOC sensor using a SnS_2 nano-lotus structure. *J. Mater. Chem. C* **2021**, *9* (24), 7713−7725.
(26) Verma, A.; Yadav, B. C. 2D/2D nanostructured system based on WO_3/WS_2 for acetone sensor and breath analyzer. *ACS Appl. Nano Mater.* **2023**, *6* (7), 5493−5507.
(27) Moura, P. C.; Ribeiro, P. A.; Raposo, M.; Vassilenko, V. The state of the art on graphene-based sensors for human health monitoring through breath biomarkers. *Sensors* **2023**, *23* (22), 9271.
(28) Ellis, J. E.; Star, A. Carbon nanotube based gas sensors toward breath analysis. *ChemPlusChem.* **2016**, *81* (12), 1248−1265.
(29) Kim, I.-D.; Rothschild, A.; Tuller, H. L. Advances and new directions in gas-sensing devices. *Acta Mater.* **2013**, *61* (3), 974−1000.
(30) Baek, J. W.; Kim, I.-D. Advances in Perovskite Oxides for Chemiresistive Sensors. *Acc. Mater. Res.* **2023**, *4* (12), 1108−1120.
(31) Di Natale, C.; Paolesse, R.; Martinelli, E.; Capuano, R. Solid-state gas sensors for breath analysis: A review. *Anal. Chim. Acta* **2014**, *824*, 1−17.
(32) Shetty, S. S.; Jayarama, A.; Karunasagar, I.; Pinto, R. A review on chemi-resistive human exhaled breath biosensors for early diagnosis of disease. *Mater. Today: Proc.* **2022**, *55*, 122−126.
(33) Yoon, J.-W.; Lee, J.-H. Toward breath analysis on a chip for disease diagnosis using semiconductor-based chemiresistors: Recent progress and future perspectives. *Lab Chip* **2017**, *17* (21), 3537−3557.
(34) Barsan, N.; Weimar, U. Conduction model of metal oxide gas sensors. *J. Electroceram.* **2001**, *7*, 143−167.
(35) Korotcenkov, G.; Cho, B. Engineering approaches to improvement of conductometric gas sensor parameters. Part 2: Decrease of dissipated (consumable) power and improvement stability and reliability. *Sens. Actuators, B* **2014**, *198*, 316−341.
(36) Majhi, S. M.; Mirzaei, A.; Kim, H. W.; Kim, S. S.; Kim, T. W. Recent advances in energy-saving chemiresistive gas sensors: A review. *Nano Energy* **2021**, *79*, No. 105369.
(37) Hulanicki, A.; Glab, S.; Ingman, F. Chemical sensors: definitions and classification. *Pure Appl. Chem.* **1991**, *63* (9), 1247−1250.
(38) Barsan, N.; Koziej, D.; Weimar, U. Metal oxide-based gas sensor research: How to? *Sens. Actuators, B* **2007**, *121* (1), 18−35.
(39) Bârsan, N.; Hübner, M.; Weimar, U. Conduction mechanisms in SnO_2 based polycrystalline thick film gas sensors exposed to CO and H_2 in different oxygen backgrounds. *Sens. Actuators, B* **2011**, *157* (2), 510−517.
(40) Degler, D.; Weimar, U.; Barsan, N. Current understanding of the fundamental mechanisms of doped and loaded semiconducting metal-oxide-based gas sensing materials. *ACS Sens.* **2019**, *4* (9), 2228−2249.
(41) Müller, S. A.; Degler, D.; Feldmann, C.; Türk, M.; Moos, R.; Fink, K.; Studt, F.; Gerthsen, D.; Bârsan, N.; Grunwaldt, J. D. Exploiting synergies in catalysis and gas sensing using noble metal-loaded oxide composites. *ChemCatChem.* **2018**, *10* (5), 864−880.
(42) Kim, S. J.; Choi, S. J.; Jang, J. S.; Cho, H. J.; Koo, W. T.; Tuller, H. L.; Kim, I.-D. Exceptional high-performance of Pt-based bimetallic catalysts for exclusive detection of exhaled biomarkers. *Adv. Mater.* **2017**, *29* (36), 1700737.
(43) Moseley, P. T. Progress in the development of semiconducting metal oxide gas sensors: a review. *Meas. Sci. Technol.* **2017**, *28* (8), No. 082001.
(44) Zhu, L.-Y.; Ou, L.-X.; Mao, L.-W.; Wu, X.-Y.; Liu, Y.-P.; Lu, H.-L. Advances in noble metal-decorated metal oxide nanomaterials for chemiresistive gas sensors: overview. *Nano-Micro Lett.* **2023**, *15* (1), 89.
(45) Hansen, T. W.; DeLaRiva, A. T.; Challa, S. R.; Datye, A. K. Sintering of catalytic nanoparticles: particle migration or Ostwald ripening? *Acc. Chem. Res.* **2013**, *46* (8), 1720−1730.
(46) McFarland, E. W.; Metiu, H. Catalysis by doped oxides. *Chem. Rev.* **2013**, *113* (6), 4391−4427.
(47) Lei, G.; Pan, H.; Mei, H.; Liu, X.; Lu, G.; Lou, C.; Li, Z.; Zhang, J. Emerging single atom catalysts in gas sensors. *Chem. Soc. Rev.* **2022**, *51* (16), 7260−7280.
(48) Yu, W.; Porosoff, M. D.; Chen, J. G. Review of Pt-based bimetallic catalysis: from model surfaces to supported catalysts. *Chem. Rev.* **2012**, *112* (11), 5780−5817.
(49) Xin, Y.; Li, S.; Qian, Y.; Zhu, W.; Yuan, H.; Jiang, P.; Guo, R.; Wang, L. High-entropy alloys as a platform for catalysis: progress, challenges, and opportunities. *ACS Catal.* **2020**, *10* (19), 11280−11306.
(50) Kim, J. H.; Kim, J. K.; Liu, J.; Curcio, A.; Jang, J.-S.; Kim, I.-D.; Ciucci, F.; Jung, W. Nanoparticle exsolution for supported catalysts: materials design, mechanism and future perspectives. *ACS Nano* **2021**, *15* (1), 81−110.
(51) van den Broek, J.; Weber, I. C.; Güntner, A. T.; Pratsinis, S. E. Highly selective gas sensing enabled by filters. *Mater. Horiz.* **2021**, *8* (3), 661−684.
(52) Postica, V.; Vahl, A.; Strobel, J.; Santos-Carballal, D.; Lupan, O.; Cadi-Essadek, A.; de Leeuw, N. H.; Schutt, F.; Polonskyi, O.; Strunskus, T.; Baum, M.; Kienle, L.; Adelung, R.; Faupel, F. Tuning doping and surface functionalization of columnar oxide films for volatile organic compound sensing: experiments and theory. *J. Mater. Chem. A* **2018**, *6* (46), 23669−23682.
(53) Song, L.; Xu, L.; Ahn, J.; Baek, J. W.; Kim, I.-D. Surface Modulation of Co_3O_4 Yolk−Shell Spheres with Tungsten Doping for Superior Acetone Sensitivity. *ACS Sens.* **2023**, *8* (9), 3417−3427.

https://doi.org/10.1021/acssensors.4c02464
ACS Sens. 2025, 10, 33−53

(54) Chu, T.; Rong, C.; Zhou, L.; Mao, X.; Zhang, B.; Xuan, F. Progress and perspectives of single-atom catalysts for gas sensing. *Adv. Mater.* **2023**, *35* (3), 2206783.
(55) Liu, Y.; Zhu, L.-Y.; Feng, P.; Dang, C.; Li, M.; Lu, H.-L.; Gao, L. Bimetallic AuPt alloy nanoparticles decorated on ZnO nanowires towards efficient and selective H_2S gas sensing. *Sens. Actuators, B* **2022**, *367*, No. 132024.
(56) V, J.; Mishra, S. S.; MB, K. U.; Thomas, S. P; Tiwary, C. S.; Biswas, K.; Kamble, V. B. Highly Sensitive and Selective Triethylamine Sensing through High-Entropy Alloy (Ti-Zr-Cr-V-Ni) Nanoparticle-Induced Fermi Energy Control of MoS_2 Nanosheets. *ACS Appl. Mater. Interfaces* **2022**, *14* (11), 13653−13664.
(57) Sharma, B.; Kumar, M.; Sharma, A. In situ ex-solution of CoFeRu solid solution nanoparticles from non-stoichiometric $(La_{0.8}Sr_{0.2})_{0.9}Co_{0.1}Fe_{0.8}Ru_{0.1}O_{3-\delta}$ perovskite for hydrogen gas sensor. *Sens. Actuators, B* **2025**, *422*, No. 136529.
(58) Güntner, A. T.; Weber, I. C.; Pratsinis, S. E. Catalytic filter for continuous and selective ethanol removal prior to gas sensing. *ACS Sens.* **2020**, *5* (4), 1058−1067.
(59) Wang, X.; Sun, G.; Routh, P.; Kim, D.-H.; Huang, W.; Chen, P. Heteroatom-doped graphene materials: syntheses, properties and applications. *Chem. Soc. Rev.* **2014**, *43* (20), 7067−7098.
(60) Yamazoe, N.; Kurokawa, Y.; Seiyama, T. Effects of additives on semiconductor gas sensors. *Sens. Actuators* **1983**, *4*, 283−289.
(61) Kaushal, S.; Kaur, M.; Kaur, N.; Kumari, V.; Singh, P. P. Heteroatom-doped graphene as sensing materials: A mini review. *RSC Adv.* **2020**, *10* (48), 28608−28629.
(62) Choi, S. J.; Yu, H.; Jang, J. S.; Kim, M. H.; Kim, S. J.; Jeong, H. S.; Kim, I.-D. Nitrogen-doped single graphene fiber with platinum water dissociation catalyst for wearable humidity sensor. *Small* **2018**, *14* (13), No. 1703934.
(63) Koo, W.T.; Cha, J.H.; Jung, J.W.; Choi, S.J.; Jang, J.S.; Kim, D.H.; Kim, I.D. Few-layered WS_2 nanoplates confined in Co, N-doped hollow carbon nanocages: Abundant WS_2 edges for highly sensitive gas sensors. *Adv. Funct. Mater.* **2018**, *28* (36), No. 1802575.
(64) Choi, H.-J.; Choi, S.-J.; Choo, S.; Kim, I.-D.; Lee, H. Hierarchical ZnO nanowires-loaded Sb-doped SnO_2-ZnO micrograting pattern via direct imprinting-assisted hydrothermal growth and its selective detection of acetone molecules. *Sci. Rep.* **2016**, *6* (1), 18731.
(65) Park, H.; Kim, D. H.; Ma, B. S.; Shin, E.; Kim, Y.; Kim, T. S.; Kim, F. S.; Kim, I.-D.; Kim, B. J. High-Performance, Flexible NO_2 Chemiresistors Achieved by Design of Imine-Incorporated n-Type Conjugated Polymers. *Adv. Sci.* **2022**, *9* (14), No. 2200270.
(66) Ma, Z.; Shi, W.; Yan, K.; Pan, L.; Yu, G. Doping engineering of conductive polymer hydrogels and their application in advanced sensor technologies. *Chem. Sci.* **2019**, *10* (25), 6232−6244.
(67) Al-Hashem, M.; Akbar, S.; Morris, P. Role of oxygen vacancies in nanostructured metal-oxide gas sensors: a review. *Sens. Actuators, B* **2019**, *301*, No. 126845.
(68) Dey, A. Semiconductor metal oxide gas sensors: A review. *Mater. Sci. Eng., B* **2018**, *229*, 206−217.
(69) Wu, J.; Huang, Q.; Zeng, D.; Zhang, S.; Yang, L.; Xia, D.; Xiong, Z.; Xie, C. Al-doping induced formation of oxygen-vacancy for enhancing gas-sensing properties of SnO_2 NTs by electrospinning. *Sens. Actuators, B* **2014**, *198*, 62−69.
(70) Jiang, Z.; Zhao, R.; Sun, B.; Nie, G.; Ji, H.; Lei, J.; Wang, C. Highly sensitive acetone sensor based on Eu-doped SnO_2 electrospun nanofibers. *Ceram. Int.* **2016**, *42* (14), 15881−15888.
(71) Lee, H.; Paeng, K.; Kim, I. S. A review of doping modulation in graphene. *Synth. Met.* **2018**, *244*, 36−47.
(72) Johannsen, J. C.; Ulstrup, S.; Crepaldi, A.; Cilento, F.; Zacchigna, M.; Miwa, J. A.; Cacho, C.; Chapman, R. T.; Springate, E.; Fromm, F. Tunable carrier multiplication and cooling in graphene. *Nano Lett.* **2015**, *15* (1), 326−331.
(73) Wei, D.; Liu, Y.; Wang, Y.; Zhang, H.; Huang, L.; Yu, G. Synthesis of N-doped graphene by chemical vapor deposition and its electrical properties. *Nano Lett.* **2009**, *9* (5), 1752−1758.
(74) Nie, L.; Mei, D.; Xiong, H.; Peng, B.; Ren, Z.; Hernandez, X. I. P.; DeLaRiva, A.; Wang, M.; Engelhard, M. H.; Kovarik, L. Activation of surface lattice oxygen in single-atom Pt/CeO_2 for low-temperature CO oxidation. *Science* **2017**, *358* (6369), 1419−1423.
(75) Lee, B.-H.; Park, S.; Kim, M.; Sinha, A. K.; Lee, S. C.; Jung, E.; Chang, W. J.; Lee, K.-S.; Kim, J. H.; Cho, S.-P. Reversible and cooperative photoactivation of single-atom Cu/TiO_2 photocatalysts. *Nat. Mater.* **2019**, *18* (6), 620−626.
(76) Shin, H.; Jung, W.-G.; Kim, D.-H.; Jang, J.-S.; Kim, Y. H.; Koo, W.-T.; Bae, J.; Park, C.; Cho, S.-H.; Kim, B. J.; Kim, I.-D. Single-atom Pt stabilized on one-dimensional nanostructure support via carbon nitride/SnO_2 heterojunction trapping. *ACS Nano* **2020**, *14* (9), 11394−11405.
(77) Shin, H.; Ko, J.; Park, C.; Kim, D. H.; Ahn, J.; Jang, J. S.; Kim, Y. H.; Cho, S. H.; Baik, H.; Kim, I.-D. Sacrificial template-assisted synthesis of inorganic nanosheets with high-loading single-atom catalysts: a general approach. *Adv. Funct. Mater.* **2022**, *32* (12), No. 2110485.
(78) Rybin, M.; Pereyaslavtsev, A.; Vasilieva, T.; Myasnikov, V.; Sokolov, I.; Pavlova, A.; Obraztsova, E.; Khomich, A.; Ralchenko, V.; Obraztsova, E. Efficient nitrogen doping of graphene by plasma treatment. *Carbon* **2016**, *96*, 196−202.
(79) Tang, Y.-B.; Yin, L.-C.; Yang, Y.; Bo, X.-H.; Cao, Y.-L.; Wang, H.-E.; Zhang, W.-J.; Bello, I.; Lee, S.-T.; Cheng, H.-M. Tunable band gaps and p-type transport properties of boron-doped graphenes by controllable ion doping using reactive microwave plasma. *ACS Nano* **2012**, *6* (3), 1970−1978.
(80) Liu, H.; Liu, Y.; Zhu, D. Chemical doping of graphene. *J. Mater. Chem.* **2011**, *21* (10), 3335−3345.
(81) Miao, X.; Tongay, S.; Petterson, M. K.; Berke, K.; Rinzler, A. G.; Appleton, B. R.; Hebard, A. F. High efficiency graphene solar cells by chemical doping. *Nano Lett.* **2012**, *12* (6), 2745−2750.
(82) Kim, D.-H.; Cha, J.-H.; Chong, S.; Cho, S.-H.; Shin, H.; Ahn, J.; Jeon, D.; Kim, J.; Choi, S.-Y.; Kim, I.-D. Flash-Thermal Shock Synthesis of Single Atoms in Ambient Air. *ACS Nano* **2023**, *17* (23), 23347−23358.
(83) Cha, J. H.; Kim, D. H.; Park, C.; Choi, S. J.; Jang, J. S.; Yang, S. Y.; Kim, I.-D.; Choi, S. Y. Low-thermal-budget doping of 2D materials in ambient air exemplified by synthesis of boron-doped reduced graphene oxide. *Adv. Sci.* **2020**, *7* (7), No. 1903318.
(84) Singh, A. K.; Xu, Q. Synergistic catalysis over bimetallic alloy nanoparticles. *ChemCatChem.* **2013**, *5* (3), 652−676.
(85) Jacobsen, C. J.; Dahl, S.; Clausen, B. S.; Bahn, S.; Logadottir, A.; Nørskov, J. K. Catalyst design by interpolation in the periodic table: bimetallic ammonia synthesis catalysts. *J. Am. Chem. Soc.* **2001**, *123* (34), 8404−8405.
(86) Kalantar-Zadeh, K.; Berean, K. J.; Burgell, R. E.; Muir, J. G.; Gibson, P. R. Intestinal gases: influence on gut disorders and the role of dietary manipulations. *Nat. Rev. Gastroenterol. Hepatol.* **2019**, *16* (12), 733−747.
(87) Koo, W.-T.; Cho, H.-J.; Kim, D.-H.; Kim, Y. H.; Shin, H.; Penner, R. M.; Kim, I.-D. Chemiresistive hydrogen sensors: fundamentals, recent advances, and challenges. *ACS Nano* **2020**, *14* (11), 14284−14322.
(88) Van Tran, T.; Kim, D.-S.; Le, T. D.; Oh, G.-J.; Shin, G.-S.; Yu, Y.-T. Alloy core composition effect of Pd-$Au_{gr\text{-}alloy}$@ZnO core−shell nanoparticles on hydrogen gas sensing performance. *Chem. Eng. J.* **2024**, *483*, No. 149050.
(89) Pandey, G.; Lawaniya, S. D.; Kumar, S.; Dwivedi, P. K.; Awasthi, K. A highly selective, efficient hydrogen gas sensor based on bimetallic (Pd−Au) alloy nanoparticle (NP)-decorated SnO_2 nanorods. *J. Mater. Chem. A* **2023**, *11* (48), 26687−26697.
(90) Le, H.-J.; Van Dao, D.; Yu, Y.-T. Superfast and efficient hydrogen gas sensor using $PdAu_{alloy}$@ZnO core−shell nanoparticles. *J. Mater. Chem. A* **2020**, *8* (26), 12968−12974.
(91) Ahemad, M. J.; Le, T. D.; Kim, D.-S.; Yu, Y.-T. Bimetallic $AgAu_{alloy}$@ZnO core-shell nanoparticles for ultra-high detection of ethanol: Potential impact of alloy composition on sensing performance. *Sens. Actuators, B* **2022**, *359*, No. 131595.

https://doi.org/10.1021/acssensors.4c02464
ACS Sens. 2025, 10, 33−53

(92) Xu, Y.; Ruban, A. V.; Mavrikakis, M. Adsorption and dissociation of O_2 on Pt−Co and Pt− Fe alloys. *J. Am. Chem. Soc.* **2004**, *126* (14), 4717−4725.
(93) Ramgir, N. S.; Mulla, I. S.; Vijayamohanan, K. P. A room temperature nitric oxide sensor actualized from Ru-doped SnO_2 nanowires. *Sens. Actuators, B* **2005**, *107* (2), 708−715.
(94) Park, C.; Koo, W. T.; Chong, S.; Shin, H.; Kim, Y. H.; Cho, H. J.; Jang, J. S.; Kim, D. H.; Lee, J.; Park, S.; Ko, J.; Kim, J.; Kim, I.-D. Confinement of Ultrasmall Bimetallic Nanoparticles in Conductive Metal−Organic Frameworks via Site-Specific Nucleation. *Adv. Mater.* **2021**, *33* (38), No. 2101216.
(95) Yeh, J. W.; Chen, S. K.; Lin, S. J.; Gan, J. Y.; Chin, T. S.; Shun, T. T.; Tsau, C. H.; Chang, S. Y. Nanostructured high-entropy alloys with multiple principal elements: novel alloy design concepts and outcomes. *Adv. Eng. Mater.* **2004**, *6* (5), 299−303.
(96) George, E. P.; Raabe, D.; Ritchie, R. O. High-entropy alloys. *Nat. Rev. Mater.* **2019**, *4* (8), 515−534.
(97) Nellaiappan, S.; Katiyar, N. K.; Kumar, R.; Parui, A.; Malviya, K. D.; Pradeep, K.; Singh, A. K.; Sharma, S.; Tiwary, C. S.; Biswas, K. High-entropy alloys as catalysts for the CO_2 and CO reduction reactions: experimental realization. *ACS Catal.* **2020**, *10* (6), 3658−3663.
(98) Wang, B.; Wang, C.; Yu, X.; Cao, Y.; Gao, L.; Wu, C.; Yao, Y.; Lin, Z.; Zou, Z. General synthesis of high-entropy alloy and ceramic nanoparticles in nanoseconds. *Nat., Synth.* **2022**, *1* (2), 138−146.
(99) Urs, K. M.; Katiyar, N. K.; Kumar, R.; Biswas, K.; Singh, A. K.; Tiwary, C.; Kamble, V. Multi-component (Ag−Au−Cu−Pd−Pt) alloy nanoparticle-decorated p-type 2D-molybdenum disulfide (MoS_2) for enhanced hydrogen sensing. *Nanoscale* **2020**, *12* (22), 11830−11841.
(100) Mondal, B.; Zhang, X.; Kumar, S.; Long, F.; Katiyar, N. K.; Kumar, M.; Goel, S.; Biswas, K. A resistance-driven H_2 gas sensor: high-entropy alloy nanoparticles decorated 2D MoS_2. *Nanoscale* **2023**, *15* (42), 17097−17104.
(101) Kwon, O.; Joo, S.; Choi, S.; Sengodan, S.; Kim, G. Review on exsolution and its driving forces in perovskites. *JPhys. Energy* **2020**, *2* (3), No. 032001.
(102) Kim, Y. H.; Jeong, H.; Won, B.-R.; Jeon, H.; Park, C.-h.; Park, D.; Kim, Y.; Lee, S.; Myung, J.-h. Nanoparticle Exsolution on Perovskite Oxides: Insights into Mechanism, Characteristics and Novel Strategies. *Nano-Micro Lett.* **2024**, *16* (1), 33.
(103) Li, X.; Dai, L.; He, Z.; Meng, W.; Li, Y.; Wang, L. Enhancing NH_3 sensing performance of mixed potential type sensors by chemical exsolution of Ag nanoparticle on $AgNbO_3$ sensing electrode. *Sens. Actuators, B* **2019**, *298*, No. 126854.
(104) Meng, W.; Wu, S.; Dai, L.; Li, Y.; Wang, M.; Wang, L. An impedancemetric NH_3 sensor based on Ag nanoparticle decorated $NiFe_2O_4$ sensing electrode prepared by electrochemical exsolution method. *Sens. Actuators, B* **2024**, *414*, No. 135933.
(105) Li, X.; Dai, L.; He, Z.; Meng, W.; Li, Y.; Wang, L. In situ exsolution of PdO nanoparticles from non-stoichiometric LaFeP-$d_{0.05}O_{3+\delta}$ electrode for impedancemetric NO_2 sensor. *Sens. Actuators, B* **2019**, *298*, No. 126827.
(106) Kim, S. H.; Jeong, H.; Sharma, B.; Myung, J.-h. In situ exsolution catalyst: an innovative approach to develop highly selective and sensitive gas sensors. *ACS Appl. Mater. Interfaces* **2022**, *14* (16), 18275−18282.
(107) Jang, J. S.; Kim, J. K.; Kim, K.; Jung, W. G.; Lim, C.; Kim, S.; Kim, D. H.; Kim, B. J.; Han, J. W.; Jung, W.; Kim, I.-D. Dopant-Driven Positive Reinforcement in Ex-Solution Process: New Strategy to Develop Highly Capable and Durable Catalytic Materials. *Adv. Mater.* **2020**, *32* (46), No. 2003983.
(108) Shin, E.; Kim, D.-H.; Cha, J.-H.; Yun, S.; Shin, H.; Ahn, J.; Jang, J.-S.; Baek, J. W.; Park, C.; Ko, J.; Park, S.; Choi, S.-Y.; Kim, I.-D. Ultrafast ambient-air exsolution on metal oxide via momentary photothermal effect. *ACS Nano* **2022**, *16* (11), 18133−18142.
(109) Kim, D.-H.; Kim, J. K.; Oh, D.; Park, S.; Kim, Y. B.; Ko, J.; Jung, W.; Kim, I.-D. Exsolution hybrids functionalized on oxide nanofibers for highly active and durable catalytic materials. *ACS Nano* **2023**, *17* (6), 5842−5851.
(110) Oliaee, S.; Khodadadi, A.; Mortazavi, Y.; Alipour, S. Highly selective Pt/SnO_2 sensor to propane or methane in presence of CO and ethanol, using gold nanoparticles on Fe_2O_3 catalytic filter. *Sens. Actuators, B* **2010**, *147* (2), 400−405.
(111) Graunke, T.; Wöllenstein, J. Effects on implemented pre-heated foamed ceramic filters. *Procedia Eng.* **2012**, *47*, 506−509.
(112) Jońca, J.; Ryzhikov, A.; Fajerwerg, K.; Kahn, M. L.; Chaudret, B.; Chapelle, A.; Menini, P.; Fau, P. A novel SnO_2 sensor and its selectivity improvement with catalytic filter. *Procedia Eng.* **2014**, *87*, 923−926.
(113) Jotca, J.; Harmel, J.; Joanny, L.; Ryzhikov, A.; Kahn, M. L.; Fau, P.; Chaudret, B.; Fajerwerg, K. Au/MOx (M= Zn, Ti) nanocomposites as highly efficient catalytic filters for chemical gas sensing at room temperature and in humid atmosphere. *Sens. Actuators, B* **2017**, *249*, 357−363.
(114) Weber, I. C.; Braun, H. P.; Krumeich, F.; Güntner, A. T.; Pratsinis, S. E. Superior acetone selectivity in gas mixtures by catalyst-filtered chemoresistive sensors. *Adv. Sci.* **2020**, *7* (19), No. 2001503.
(115) Moon, Y. K.; Jeong, S.-Y.; Kang, Y. C.; Lee, J.-H. Metal oxide gas sensors with Au nanocluster catalytic overlayer: toward tuning gas selectivity and response using a novel bilayer sensor design. *ACS Appl. Mater. Interfaces* **2019**, *11* (35), 32169−32177.
(116) Zhou, Q.; Xu, L.; Kan, Z.; Yang, L.; Chang, Z.; Dong, B.; Bai, X.; Lu, G.; Song, H. A multi-platform sensor for selective and sensitive H_2S monitoring: three-dimensional macroporous ZnO encapsulated by MOFs with small Pt nanoparticles. *J. Hazard. Mater.* **2022**, *426*, No. 128075.
(117) Park, C.-O.; Akbar, S.; Hwang, J. Selective gas detection with catalytic filter. *Mater. Chem. Phys.* **2002**, *75* (1−3), 56−60.
(118) Moon, Y. K.; Jeong, S. Y.; Jo, Y. M.; Jo, Y. K.; Kang, Y. C.; Lee, J. H. Highly selective detection of benzene and discrimination of volatile aromatic compounds using oxide chemiresistors with tunable $Rh-TiO_2$ catalytic overlayers. *Adv. Sci.* **2021**, *8* (6), No. 2004078.
(119) Dou, S.; Xu, J.; Cui, X.; Liu, W.; Zhang, Z.; Deng, Y.; Hu, W.; Chen, Y. High-temperature shock enabled nanomanufacturing for energy-related applications. *Adv. Energy Mater.* **2020**, *10* (33), No. 2001331.
(120) Yao, Y.; Huang, Z.; Xie, P.; Lacey, S. D.; Jacob, R. J.; Xie, H.; Chen, F.; Nie, A.; Pu, T.; Rehwoldt, M.; Yu, D.; Zachariah, M.; Wang, C.; Yassar, R.; Lu, J.; Hu, L. Carbothermal shock synthesis of high-entropy-alloy nanoparticles. *Science* **2018**, *359* (6383), 1489−1494.
(121) Wyss, K. M.; Luong, D. X.; Tour, J. M. Large-scale syntheses of 2D materials: flash joule heating and other methods. *Adv. Mater.* **2022**, *34* (8), No. 2106970.
(122) Choi, S.-J.; Kim, S.-J.; Kim, I.-D. Ultrafast optical reduction of graphene oxide sheets on colorless polyimide film for wearable chemical sensors. *NPG Asia Mater.* **2016**, *8* (9), e315−e315.
(123) Choi, S.-J.; Kim, S. J.; Jang, J. S.; Lee, J. H.; Kim, I.-D. Silver nanowire embedded colorless polyimide heater for wearable chemical sensors: improved reversible reaction kinetics of optically reduced graphene oxide. *Small* **2016**, *12* (42), 5826−5835.
(124) Choi, S.-J.; Jang, J. S.; Park, H. J.; Kim, I.-D. Optically sintered 2D RuO_2 nanosheets: temperature-controlled NO_2 reaction. *Adv. Funct. Mater.* **2017**, *27* (13), No. 1606026.
(125) Cui, X.; Ruan, Q.; Zhuo, X.; Xia, X.; Hu, J.; Fu, R.; Li, Y.; Wang, J.; Xu, H. Photothermal nanomaterials: a powerful light-to-heat converter. *Chem. Rev.* **2023**, *123* (11), 6891−6952.
(126) Kim, D.-H.; Cha, J.-H.; Shim, G.; Kim, Y. H.; Jang, J.-S.; Shin, H.; Ahn, J.; Choi, S.-Y.; Kim, I.-D. Flash-thermochemical engineering of phase and surface activity on metal oxides. *Chem.* **2022**, *8* (4), 1014−1033.
(127) Chae, S.; Ahn, J.; Nam, J. S.; Jang, J.-S.; Kim, I.-D. Thermal shock-stabilized metal catalysts on oxide hemitubes: Toward ultra-sensitive chemiresistors. *Appl. Surf. Sci.* **2022**, *595*, No. 153460.
(128) Zhao, J.; Yi, N.; Ding, X.; Liu, S.; Zhu, J.; Castonguay, A. C.; Gao, Y.; Zarzar, L. D.; Cheng, H. In situ laser-assisted synthesis and

patterning of graphene foam composites as a flexible gas sensing platform. *Chem. Eng. J.* **2023**, *456*, No. 140956.
(129) Mou, T.; Pillai, H. S.; Wang, S.; Wan, M.; Han, X.; Schweitzer, N. M.; Che, F.; Xin, H. Bridging the complexity gap in computational heterogeneous catalysis with machine learning. *Nat. Catal.* **2023**, *6* (2), 122−136.
(130) Kim, M.; Kim, Y.; Ha, M. Y.; Shin, E.; Kwak, S. J.; Park, M.; Kim, I.-D.; Jung, W. B.; Lee, W. B.; Kim, Y. Exploring optimal water splitting bifunctional alloy catalyst by pareto active learning. *Adv. Mater.* **2023**, *35* (17), No. 2211497.
(131) Kim, M.; Ha, M. Y.; Jung, W. B.; Yoon, J.; Shin, E.; Kim, I.-D.; Lee, W. B.; Kim, Y.; Jung, H. T. Searching for an optimal multi-metallic alloy catalyst by active learning combined with experiments. *Adv. Mater.* **2022**, *34* (19), No. 2108900.
(132) Ghosal, S.; Dey, S.; Bhattacharyya, P.; Chattopadhyay, P. P.; Datta, S. Data-driven design of ternary alloy catalysts for enhanced oxide-based gas sensors' performance. *Comput. Mater. Sci.* **2019**, *161*, 255−260.
(133) Chen, J.; Chen, Z.; Boussaid, F.; Zhang, D.; Pan, X.; Zhao, H.; Bermak, A.; Tsui, C.-Y.; Wang, X.; Fan, Z. Ultra-low-power smart electronic nose system based on three-dimensional tin oxide nanotube arrays. *ACS Nano* **2018**, *12* (6), 6079−6088.
(134) Li, Y.; Wei, X.; Zhou, Y.; Wang, J.; You, R. Research progress of electronic nose technology in exhaled breath disease analysis. *Microsyst. Nanoeng.* **2023**, *9* (1), 129.
(135) Chen, Z.; Chen, Z.; Song, Z.; Ye, W.; Fan, Z. Smart gas sensor arrays powered by artificial intelligence. *J. Semicond.* **2019**, *40* (11), No. 111601.
(136) Liu, B.; Huang, Y.; Kam, K. W.; Cheung, W.-F.; Zhao, N.; Zheng, B. Functionalized graphene-based chemiresistive electronic nose for discrimination of disease-related volatile organic compounds. *J. Biosens. Bioelectron.* **2019**, *1*, No. 100016.
(137) Marzorati, D.; Mainardi, L.; Sedda, G.; Gasparri, R.; Spaggiari, L.; Cerveri, P. A metal oxide gas sensors array for lung cancer diagnosis through exhaled breath analysis. In *2019 41st Annual International Conference of the IEEE Engineering in Medicine and Biology Society (EMBC)*, 2019; IEEE: pp 1584−1587.
(138) Tenero, L.; Sandri, M.; Piazza, M.; Paiola, G.; Zaffanello, M.; Piacentini, G. Electronic nose in discrimination of children with uncontrolled asthma. *J. Breath Res.* **2020**, *14* (4), No. 046003.
(139) van Keulen, K. E.; Jansen, M. E.; Schrauwen, R. W.; Kolkman, J. J.; Siersema, P. D. Volatile organic compounds in breath can serve as a non-invasive diagnostic biomarker for the detection of advanced adenomas and colorectal cancer. *Aliment. Pharmacol. Ther.* **2020**, *51* (3), 334−346.
(140) Oh, J.; Kim, S. H.; Lee, M.-J.; Hwang, H.; Ku, W.; Lim, J.; Hwang, I.-S.; Lee, J.-H.; Hwang, J.-H. Machine learning-based discrimination of indoor pollutants using an oxide gas sensor array: High endurance against ambient humidity and temperature. *Sens. Actuators, B* **2022**, *364*, No. 131894.
(141) Singh, S.; S, S.; Varma, P.; Sreelekha, G.; Adak, C.; Shukla, R. P.; Kamble, V. B. Metal oxide-based gas sensor array for VOCs determination in complex mixtures using machine learning. *Microchim. Acta* **2024**, *191* (4), 196.
(142) Sung, S.-H.; Suh, J. M.; Hwang, Y. J.; Jang, H. W.; Park, J. G.; Jun, S. C. Data-centric artificial olfactory system based on the eigengraph. *Nat. Commun.* **2024**, *15* (1), 1211.
(143) Chen, Q.; Chen, Z.; Liu, D.; He, Z.; Wu, J. Constructing an E-nose using metal-ion-induced assembly of graphene oxide for diagnosis of lung cancer via exhaled breath. *ACS Appl. Mater. Interfaces* **2020**, *12* (15), 17713−17724.
(144) Shang, G.; Dinh, D.; Mercer, T.; Yan, S.; Wang, S.; Malaei, B.; Luo, J.; Lu, S.; Zhong, C.-J. Chemiresistive sensor array with nanostructured interfaces for detection of human breaths with simulated lung cancer breath VOCs. *ACS Sens.* **2023**, *8* (3), 1328−1338.
(145) Freddi, S.; Vergari, M.; Pagliara, S.; Sangaletti, L. A Chemiresistor sensor array based on graphene nanostructures: From the detection of ammonia and possible interfering VOCs to chemometric analysis. *Sensors* **2023**, *23* (2), 882.
(146) Luo, J.; Luo, J.; Wang, L.; Shi, X.; Yin, J.; Crew, E.; Lu, S.; Lesperance, L. M.; Zhong, C.-J. Nanoparticle-structured thin film sensor arrays for breath sensing. *Sens. Actuators, B* **2012**, *161* (1), 845−854.
(147) Lee, J.; Jung, Y.; Sung, S.-H.; Lee, G.; Kim, J.; Seong, J.; Shim, Y.-S.; Jun, S. C.; Jeon, S. High-performance gas sensor array for indoor air quality monitoring: The role of Au nanoparticles on WO_3, SnO_2, and NiO-based gas sensors. *J. Mater. Chem. A* **2021**, *9* (2), 1159−1167.
(148) Freddi, S.; Emelianov, A. V.; Bobrinetskiy, I. I.; Drera, G.; Pagliara, S.; Kopylova, D. S.; Chiesa, M.; Santini, G.; Mores, N.; Moscato, U. Development of a sensing array for human breath analysis based on SWCNT layers functionalized with semiconductor organic molecules. *Adv. Healthcare Mater.* **2020**, *9* (12), No. 2000377.
(149) Duan, Q.; Zhang, W.; Li, L.; Ying, B.; Li, T.; Chen, B.; Li, H.-Y.; Liu, H. W-CeO_2 nanospheres gas sensor array for accurate and selective H_2S detection in exhaled breath. *Chem. Eng. J.* **2024**, *479*, No. 147748.
(150) Yang, H.-Y.; Wang, Y.-C.; Peng, H.-Y.; Huang, C.-H. Breath biopsy of breast cancer using sensor array signals and machine learning analysis. *Sci. Rep.* **2021**, *11* (1), 103.
(151) Li, W.; Liu, H.; Xie, D.; He, Z.; Pi, X. Lung cancer screening based on type-different sensor arrays. *Sci. Rep.* **2017**, *7* (1), 1969.
(152) Lee, K.; Cho, I.; Kang, M.; Jeong, J.; Choi, M.; Woo, K. Y.; Yoon, K.-J.; Cho, Y.-H.; Park, I. Ultra-low-power e-nose system based on multi-micro-led-integrated, nanostructured gas sensors and deep learning. *ACS Nano* **2023**, *17* (1), 539−551.
(153) Mei, H.; Peng, J.; Wang, T.; Zhou, T.; Zhao, H.; Zhang, T.; Yang, Z. Overcoming the limits of cross-sensitivity: Pattern recognition methods for chemiresistive gas sensor array. *Nano-Micro Lett.* **2024**, *16* (1), 269.
(154) Kumar, K.; Chaudhri, S. N.; Rajput, N. S.; Shvetsov, A. V.; Sahal, R.; Alsamhi, S. H. An IoT-enabled E-Nose for remote detection and monitoring of airborne pollution hazards using LoRa network protocol. *Sensors* **2023**, *23* (10), 4885.
(155) Hwang, Y. J.; Yu, H.; Lee, G.; Shackery, I.; Seong, J.; Jung, Y.; Sung, S.-H.; Choi, J.; Jun, S. C. Multiplexed DNA-functionalized graphene sensor with artificial intelligence-based discrimination performance for analyzing chemical vapor compositions. *Microsyst. Nanoeng.* **2023**, *9* (1), 28.
(156) Vapnik, V.; Golowich, S.; Smola, A. Support vector method for function approximation, regression estimation and signal processing. *Advances in neural information processing systems* **1996**, *9*.
(157) Yan, K.; Zhang, D. Feature selection and analysis on correlated gas sensor data with recursive feature elimination. *Sens. Actuators, B* **2015**, *212*, 353−363.
(158) Zhan, C.; He, J.; Pan, M.; Luo, D. Component analysis of gas mixture based on one-dimensional convolutional neural network. *Sensors* **2021**, *21* (2), 347.
(159) Baek, J. W.; Han, S.; Lee, S. E.; Ahn, J.; Park, C.; Nam, J. S.; Kim, Y. H.; Shin, E.; Kim, M.; Jang, J.-S. Cobalt-Doped Ceria Sensitizer Effects on Metal Oxide Nanofibers: Heightened Surface Reactivity for High-Performing Chemiresistive Sensors. *ACS Nano* **2024**. DOI: 10.1021/acsnano.4c03168
(160) Tian, R.; Ji, P.; Luo, Z.; Li, J.; Sun, J. Room-temperature NH_3 gas sensor based on atomically dispersed Co with a simple structure. *New J. Chem.* **2021**, *45* (23), 10240−10247.
(161) Rong, Q.; Xiao, B.; Zeng, J.; Yu, R.; Zi, B.; Zhang, G.; Zhu, Z.; Zhang, J.; Wu, J.; Liu, Q. Pt single atom-induced activation energy and adsorption enhancement for an ultrasensitive ppb-level methanol gas sensor. *ACS Sens.* **2022**, *7* (1), 199−206.
(162) Wang, Y.; Liu, Z.; Yang, L.; Li, Y.; Bai, J.; Sui, C.; Liu, Y.; Liang, X.; Liu, F.; Lu, G. Highly selective gas sensor for rapid detection of triethylamine using PdRu alloy nanoparticles functionalized SnO_2. *Sens. Actuators, B* **2023**, *379*, No. 133205.
(163) Zhou, Q.; Xu, L.; Kan, Z.; Yang, L.; Chang, Z.; Dong, B.; Bai, X.; Lu, G.; Song, H. A multi-platform sensor for selective and sensitive

H_2S monitoring: three-dimensional macroporous ZnO encapsulated by MOFs with small Pt nanoparticles. *J. Hazard. Mater.* **2022**, *426*, No. 128075.

(164) Ahn, J.; Park, S.; Oh, D.; Lim, Y.; Nam, J. S.; Kim, J.; Jung, W.; Kim, I.-D. Rapid Joule Heating Synthesis of Oxide-Socketed High-Entropy Alloy Nanoparticles as CO_2 Conversion Catalysts. *ACS Nano* **2023**, *17* (13), 12188−12199.

(165) Shin, H.; Kim, D.-H.; Jung, W.; Jang, J.-S.; Kim, Y. H.; Lee, Y.; Chang, K.; Lee, J.; Park, J.; Namkoong, K.; Kim, I.-D. Surface activity-tuned metal oxide chemiresistor: toward direct and quantitative halitosis diagnosis. *ACS Nano* **2021**, *15* (9), 14207−14217.

https://doi.org/10.1021/acssensors.4c02464
ACS Sens. 2025, 10, 33−53